# Importance of cycle timing for the function of the molecular chaperone Hsp90

Bettina K. Zierer [1)], Martin Rübbelke[1,2)], Tobias Madl[1,2,3)], Franziska Tippel[1)], Klaus Richter[1)], Michael Sattler[1,2)] and Johannes Buchner[1)]

1) Center for Integrated Protein Science Munich (CIPSM) at the Department of Chemistry Technische Universität München, Lichtenbergstr.4, 85747 Garching, Germany
2) Institute of Structural Biology, Helmholtz Zentrum München, 85764 Neuherberg, Germany
3) Institute of Molecular Biology & Biochemistry, Center of Molecular Medicine, Medical University of Graz, 8010 Graz, Austria

**Abstract**

The dimeric chaperone Hsp90 couples ATP hydrolysis with large conformational changes, which are essential for the activation of many client proteins. The structural transitions involve the N-terminal dimerization and the formation of „closed states" between the N-terminal and middle domains. Here, we used Hsp90 mutants with changes in ATPase activity and biological function as probes to address the importance of conformational cycling for Hsp90 activity. Surprisingly, we found no correlation between the speed of ATP turnover and the *in vivo* activity of Hsp90. Even mutants with almost normal ATPase activity can be lethal and mutants lacking ATPase activity can be viable. What is important is the time Hsp90 spends in specific conformational states. Specifically, a prolonged population of closed states prevents the processing of client proteins. The function of co-chaperones such as Aha1 can correct defective mutants. Thus the timing of conformational transitions and the modulation by chaperones are crucial for Hsp90 function, and not cycle speed.

## Introduction

Hsp90 is an ATP-dependent molecular chaperone that controls the fate of a large set of client proteins in maturation, trafficking and degradation[1-5]. About 20% of the proteome seems to directly or indirectly depend on Hsp90 in structure and/or function[6]. Hsp90 is a homo-dimer. Each monomer consists of an N-terminal domain (N-domain), containing the nucleotide binding pocket[7] connected via a long charged linker to the middle domain (M-domain). The C-terminal domain is responsible for dimerization[8], which is a prerequisite for efficient ATPase activity[9-11]. The last five amino acids of Hsp90 form the MEEVD-motive that serves as the binding site for a large class of co-chaperones containing a peptide-binding TPR-domain[12].

ATP binding and hydrolysis which are important for the function of Hsp90 *in vivo*[13,14] are coupled to a slow conformational cycle in which the Hsp90 dimer progresses from an N-terminally open to a closed state. The open state is V-shaped, with dimerization via the C-domains and no interaction of the N-domains[15]. In the crystal structure of Hsp90 in the presence of the non-hydrolysable ATP-analogue AMP-PNP, Hsp90 adopts a compact structure in which also the N-domains are associated[16]. The conformational changes from the open to the N-terminally closed state are rate-limiting and precede ATP hydrolysis[17,18]. A FRET-based kinetic analysis of the conformational cycle revealed that Hsp90 adopts specific intermediate states[17] before it finally reaches a fully closed state, in which ATP hydrolysis occurs. Specifically, after ATP binding the so-called ATP-lid in the Hsp90 N-domain (**Fig. 1**) changes its position. This exposes a hydrophobic patch in the N-domain which, together with its counterpart in the second monomer, stabilizes the N-terminally closed state (**Fig. 1a**)[16]. Furthermore, this unlashes the contacts with the N-terminal helix that subsequently binds to the N-domain of the second subunit within the dimer. Once the N-terminal association is achieved, the Hsp90 N-domains associate with the Hsp90 M-domains and form the active ATPase. Some of the conformational states seem iso-energetic and random fluctuations between them are possible[19,20]. Several co-chaperones target specific conformations of Hsp90 and thus reduce random structural fluctuations. In addition, they modulate specific properties of Hsp90 such as its ATPase activity. Here, we used a set of mutants in the N- and M-domains of yeast Hsp90 with reported effects on biological activity (**Table 1**) to gain insight into the importance of the timing of conformational transitions for Hsp90 functionality and client protein processing.

## Results

*Mutants in the N- and M-domains modulate the ATPase activity of Hsp90*

The conformational transition from the open to the closed state is rate-limiting in the ATPase cycle of Hsp90. We thus used a set of point mutants in the N- and M-domains with reported

effects on ATP turnover and biological activity of Hsp90 (**Table 1**) to probe the role of specific conformational rearrangements in Hsp90. According to their ATPase activities, the mutants can be classified into three categories (**Fig. 1b and Table 2**). The first class exhibits an increased turnover rate with A107N and ∆8-Hsp90 showing the strongest effect and the mutations A10T, L18R and T22I increase the ATPase activity slightly. The second class includes mutants with reduced ATPase activity such as R346S and R380A. Finally, the third class, are ATPase-deficient mutants, like E33A and D79N. For most mutants, the $K_M$-values for ATP are comparable to wildtype, in the range between 0.2 - 0.7 mM (**Table 2**). Interestingly, A107N and ∆8-Hsp90 exhibited a higher affinity with values of 0.01 and 0.07 mM, respectively, implying that in these cases alterations in the binding pocket or the enzymatic mechanism may have occurred.

Altered ATPase activities in the N- and M-domain mutants suggested that specific aspects of the conformational cycle are manipulated. For detecting specific structural alterations, we tested the ability of the co-chaperone Aha1 to accelerate the cycle by promoting the formation of the unfavorable closed conformation[17,21,22]. All variants, except E33A and D79N, were stimulated by Aha1, albeit to a different extent (**Fig. 1c and Table 2**). Interestingly, the R346S variant with inherently low ATPase activity can be stimulated to wildtype-like levels. Thus, in this variant the conformational transitions specifically accelerated by Aha1 are slower compared to the wildtype protein. In contrast, R380A, which exhibits equally slow inherent ATPase activity as R346S, can only be stimulated 2-fold, implying different rate-limiting steps of these two mutants.

*Structural effects of N-domain mutations*

All mutations did not affect the overall stability of Hsp90, as evident by similar $T_m$-values between 55 and 59°C (**Supplementary Fig. 1**). Thus, the structural integrity appears to be maintained, suggesting that the differences in ATP turnover do not originate from altered stability of the Hsp90 variants. To characterize the structural effects of mutations for the conformation of the N-domain we compared $^{1}H,^{15}N$-HSQC NMR spectra of the wildtype N-domain and seven mutants. The $^{1}H,^{15}N$-HSQC NMR spectra confirm that all mutants are folded (**Supplementary Fig. 2**) consistent with the wildtype-like thermal stability. Changes in chemical shift are plotted (**Supplementary Fig. 3**) and mapped with red spheres onto the structure of the wildtype-N-domain (PDB 1AM1) (**Fig. 2a and Supplementary Fig. 4a**).

The deletion of the first eight amino acids (Δ8) leads to substantial chemical shift changes for residues in various regions of the N-domain (**Fig. 2a**). The other mutant with strongly increased ATPase activity, A107N, exhibits more local changes in the lid and in the N-terminal helices α1 and α2. The mutations in helix α1 L18R and T22I affect the same structural elements as the lid mutation A107N (**Fig. 2a**). The third N-terminal point mutation

A10T has only little effect, but the small changes are in the same region as observed for L18R and T22I (**Supplementary Fig. 4a)**

The chemical shift changes may be explained as follows: Helix α1 is part of the N-terminal dimerization interface[16]. In the open state helix α1 and the lid are in close spatial proximity[7]. Closure of the lid and N-terminal dimerization are both coupled to ATP binding[11]. Thus, the NMR chemical shift changes in the lid mutants are consistent with a coupling of lid closure and N-terminal dimerization.

The two mutations that lack ATPase activity show distinct patterns. While the E33A mutation affects all α-helices, D79N has more local effects in the β-sheet and in the helix α2. Consistent with its role in providing direct contact to ATP[7], the mutation D79N is sufficient to abolish ATP binding[13,14]. While the D79N mutation does not affect the dimerization helix and major parts of the lid, the E33A variant, which alters a residue directly involved in ATP-hydrolysis, exhibits more widespread chemical shift changes indicating that E33 is important for the conformation and dynamics of the N-domain.

To test for the effects of nucleotide binding on the conformation of variants with notably altered ATPase activity we recorded $^{1}H,^{15}N$-HSQC spectra in the presence of AMP-PNP. As expected, D79N does not bind AMP-PNP (**Supplementary Fig. 5**). Mapping NMR chemical shift differences onto the N-domain structure shows that residues affected in A107N are surrounding the nucleotide binding site (**Fig. 2b**). For A107N, defined NMR chemical shift are seen which suggests that the ATPase activity is associated with a complex allosteric network of interactions in the N-domain. Chemical shift changes for the E33A mutant, which binds but does not hydrolyze ATP, involve the β-sheet, helix α2, and potentially the lid (although this could not be confirmed due to lack of chemical shift assignments) (**Supplementary Fig. 6**).

We also investigated to what extent the mutations may influence the interaction with the co-chaperone Aha1. Chemical shift of residues located in the binding interface between Aha1 and the N-domain (**Supplementary Fig. 2b**)[22] are not changed for A10T and D79N. In contrast, for Δ8, E33A and T22I the chemical shifts of residues located in the Aha1 binding site are affected by the mutations. For L18R and A107N large regions of the Aha1 binding surface show significant chemical shift differences. These observations correlate well with the altered effects of Aha1 on ATPase activity in the different mutants compared to the wildtype.

*Distinct steps of the conformational cycle are affected by the mutations in the N- and M-domains*

Since N-terminal contact formation is important for the conformational cycle, we probed whether the mutants affected the transition to the closed state. To this end we used a FRET-system, in which the M- and N-domains in the dimer are labeled with a donor and acceptor dye, respectively[17]. Addition of ATPγS, an ATP analogue that is only slowly hydrolyzed by

Hsp90 induces N-terminal closing, a concomitant increase in FRET efficiency and the population of the closed state of Hsp90[17] (**Fig. 3a**). All but one mutant (D79N) showed changes in FRET-efficiency in response to ATPγS, indicating that this reaction is not generally abolished by the mutations. The kinetics of conformational changes were equally fast or accelerated in mutants with increased ATPase activity, and decelerated in variants with decreased ATPase rates (R346S and R380A) (**Table 2**). This is in line with the fact that the conformational changes are the rate-limiting events during the ATPase cycle[17,18].

In the presence of ATP, the closed state of wildtype Hsp90 is only marginally populated and thus no change in the FRET signal is usually observed[17]. Several mutants behaved like the wildtype protein in the presence of ATP. However, for the mutants Δ8, T22I, E33A and R380A, we detected an increase in acceptor fluorescence as a result of ATP-induced conformational changes (**Fig. 3b and Table 2**), suggesting that in these mutants the N-terminally closed state is more favored compared to the wildtype variant and ATP may be sufficient to populate the closed conformation. Interestingly, this effect was observed for mutants with higher or lower ATPase. Thus, not the kinetics of the overall reaction is important but the specific step affected by the mutation.

*Mutants in the N- and M-domains accumulate different conformations*

Our observations indicate that these mutants move differently through the conformational cycle. To gain further insight in the closed state, we performed chase experiments by adding an excess of unlabeled wildtype Hsp90 to preformed FRET-complexes. As the disruption of the FRET-complexes is strongly influenced by the N-terminal dimerization properties of Hsp90 variants[17], this allowed us to test the stability of the closed state. In the absence of nucleotides, all variants showed kinetics with comparable half-lives (**Fig. 3c and Table 3**) implying similar dimerization properties of the C-terminal domain. When ATPγS was used to induce the closed state, all mutants, except D79N, responded with dramatically increased apparent half-lives of the FRET-complexes (**Fig. 3c and Table 3**). All variants showed a slow disruption of the FRET-complex in accordance with the slow hydrolysis of ATPγS. When the FRET-complexes were pre-incubated with ATP, the chase with unlabeled Hsp90 resulted in a dramatic increase in apparent half-lives of the FRET-complexes for the variants E33A, R380A, and Δ8, and a less pronounced effect for the variants T22I and A107N compared to Hsp90 wt. Thus, several mutants capable of hydrolyzing ATP (R380A, Δ8, T22I and A107N) accumulate N-terminally associated intermediate states under continuous cycling conditions and ongoing hydrolysis.

SAXS experiments allowed us to determine the shape of the Hsp90 variants in the absence or presence of different nucleotides. The scattering curves were transformed into interatomic distance probability profiles, *P(R)*, which relate to the overall shape of Hsp90. In the absence of nucleotides, wildtype Hsp90 adopts an open conformation characterized by a broad

distribution in the *P(R)* curve (**Fig. 4a and Table 4;** $R_g$ = 64.2 Å, $D_{max}$ = 240 Å) as previously reported for yeast Hsp90[23]; [24] and the *E. coli* homologue HtpG[20]. Most variants tested showed a wildtype-like shape in the absence of nucleotide. The only exception was the Δ8-Hsp90 deletion mutant, which adopted a partly compact state as indicated by the reduced radius of gyration ($R_g$ = 61.9 Å) and a redistribution of the *P(R)* to smaller distances. This mutant may thus be already closed to some extent even in the absence of nucleotides **(Fig. 4a)**. In the presence of ATPγS, all the analyzed variants displayed a more narrow range of distribution in the *P(R)* curves indicative of a more compact state (**Fig. 4b**). Δ8-Hsp90 is further compacted and even the hydrolysis-incompetent mutant E33A showed a compact shape similar to the wildtype protein. Thus E33A seems to be able to undergo specific conformational transitions in response to binding ATP, also consistent with the NMR chemical shift changes observed. Compared to the wildtype protein R380A and L18R, but also R346S, are less efficient in adopting the closed state. This is in line with the faster subunit exchange rates in the presence of ATPγS detected for these mutants, which also imply a decreased ability to form the closed state. In contrast, in the presence of ATP, Δ8, T22I, E33A, and A107N show a redistribution of distances in the *P(R)* curves indicating that they adopt a more compact conformation, while the wildtype protein and the L18R, R346S, R380A variants display a broader distribution of distances representing the open conformation of the chaperone (**Fig. 4c**). Thus the SAXS measurements show that several of the mutants – in particular Δ8-Hsp90, E33A and to lesser extent T22I – tend to populate closed states during the ATPase cycle under conditions where the wildtype protein does not.

*Mutations modulate the population of closed states*

We had previously observed that two different conformations with dimerized N-terminal domains exist, termed "closed-1" and "closed-2". In "closed-1" the N-domains are dimerized and the bound nucleotide is not protected against exchange, as apparently the N-M interaction is not fully formed yet[25]. The "closed-2" state instead shows trapping of the nucleotide and N-M interaction[26]. From the experiments above, it cannot be deduced which of the closed forms of Hsp90 is populated in the different variants. It is however possible to differentiate between the two closed states using the conformation-sensitive co-chaperone p23, whose binding is restricted to the fully closed state (closed-2)[16,27]. We employed analytical ultracentrifugation with fluorescence detection to monitor the binding of labeled p23 to Hsp90 (**Fig. 5**). None of the Hsp90 mutants bound p23 in the absence of nucleotides (data not shown). Instead, all mutants with the exception of D79N bound p23 in the presence of ATPγS. Interestingly, the variants L18R and R380A showed reduced p23 binding indicating a destabilization of the closed-2 state. This is in line with the faster subunit exchange rates and the less compact state detected by SAXS for the respective mutants. The Δ8-variant

exhibited increased binding to p23 consistent with the pronounced population of the closed-2 state. In the presence of ATP, p23 binding was detected only for E33A, Δ8, and T22I. The strong binding of p23 to the Hsp90-variants Δ8 and T22I in the presence of ATP confirms that these mutants accumulate a closed-2-like state under continuous cycling conditions. For E33A, the closed-2 state seems to be the final conformation reached in the presence of nucleotide, as hydrolysis cannot occur. For R380A interestingly, no p23 binding could be observed although this mutant showed detectable N-terminal dimerization in the FRET-based subunit exchange experiments. This suggests that R380A populates an intermediate state of the conformational cycle, which is distinct from the closed-2 state and might represent closed-1.

*Changes in the conformational cycle can result in loss of the biological function of Hsp90*

To investigate the biological consequences of the alterations in the conformational cycle of Hsp90, the variants were tested for their ability to support yeast viability when expressed as the sole Hsp90 source in yeast. A10T, L18R, T22I, A107N, and R346S were found to support viability in yeast (**Fig. 6a**). In agreement with previous reports the expression of the D79N and R380A variants caused lethality[13,14,28]. Interestingly, R380A and R346S display similar ATPase activity but only R346S supported viability. Surprisingly and in contrast to previous studies[13,14], we found that in our system E33A was able to sustain yeast viability, although no significant ATPase activity had been detected *in vitro*. Also unexpectedly, the Δ8 Hsp90 variant was not able to support yeast viability although it showed increased ATPase activity. These results indicate that the ATP hydrolysis alone by Hsp90 is not sufficient for the essential function of Hsp90.

Under stress conditions, we could confirm the previously reported temperature-sensitive phenotype[29] for cells expressing the T22I mutant. Several variants with altered conformational cycling (L18R, E33A, A10T) were unable to sustain viability at higher temperatures (**Fig. 6b**). Only R346S and A107N mutants behaved like the wildtype protein.

*Hsp90 chaperone function is negatively affected by mutations with increased closed state formation*

Hsp90 plays an important role in the process of DNA repair in yeast [30,31]. We investigated the influence of the Hsp90 variants on this specific endogenous function. We exposed yeast cells to UV radiation to induce DNA damage that activates Hsp90-dependent nucleotide excision repair machinery. Yeast cells expressing the L18R, T22I or E33A Hsp90 variants displayed increased sensitivity towards UV radiation-mediated damage, whereas the other tested variants (A10T, A107N and R346S) behaved like wildtype yeast cells (**Fig. 6c**).

We next tested the ability of the variants to activate the two well-established Hsp90 clients viral Src kinase (v-Src) and glucocorticoid receptor (GR). Expression and activation of the oncogenic v-Src is Hsp90-dependent and leads to a cytotoxic hyperphosphorylation of cytoplasmic proteins in yeast cells[32,33]. In the presence of wildtype Hsp90 this is manifested by the inhibition of yeast cell growth upon expression of v-Src. Specifically, the Hsp90-variants L18R, T22I, E33A showed reduced toxicity indicating impaired v-Src activation (**Fig. 7a**), while the other Hsp90 variants tested (A10T, A107N and R346S) exhibited wt-like v-Src maturation. To assess GR activation, we used a β-galactosidase-based reporter assay[29]. GR processing was compromised in cells expressing the A107N variant (**Fig. 7b**). For A10T, T22I, E33A variants we detected only minor changes (15% reduction) in GR maturation, while R346S and L18R supported wildtype-like maturation of GR. Thus of the functional mutations, in particular the variants E33A and T22I appear to broadly affect client protein turnover.

To determine the reasons for these observations we looked at differences in client protein interactions. To this end, we performed analytical ultracentrifugation with GR. As recently shown, GR interacts with yeast Hsp90 in the presence and absence of nucleotides but shows a higher affinity towards ATP-complexed Hsp90[24]. We first tested the interaction of GR in the presence of ATP (**Fig. 7c,d**). Here, D79N showed the weakest affinity for GR as expected from its deficiency to bind nucleotide, while other mutants were wildtype-like. Surprisingly, the Δ8 variant exhibited strongly reduced GR binding. Furthermore, E33A and to a lesser extent T22I mutants showed partly disrupted GR binding in the presence of ATP, implying that in particular the mutants, which accumulate a closed-2 state in the presence of ATP, show weaker client interactions. In the absence of nucleotide all mutants interacted very similarly with GR irrespective of the mutations (**Figure 7e,f**). Only Δ8-Hsp90 bound strongly to the client protein implying that in this deletion mutant the GR-interacting state is already accumulated even in the absence of ATP. This is particularly interesting, as the Δ8-Hsp90 is the only variant with stronger N-terminal dimerization in the absence of ATP.

Thus, the closed state in the absence of nucleotides in Δ8-Hsp90 may represent the closed-1 state with high affinity to the receptor, while the addition of ATP induces closed-2, which binds much weaker, putting the client protein into a position to influence the turnover of the ATPase cycle.

## Discussion

In this study we used a set of Hsp90 mutants that exhibit defined changes in ATP hydrolysis, biological function and client binding. These mutants are useful tools for uncovering the mechanism of this complex molecular machine, which is characterized by large and slow conformational transitions (**Fig. 8a**). In this respect, the association of the N-terminal domains to form the closed-1 state and the subsequent interaction of the N- and M-domains to form the closed-2 state are of importance as these processes represent the rate limiting steps of the ATP hydrolysis cycle. The mutations studied affect structural elements involved in the conformational changes leading to the active ATPase conformation. Specifically, they are located in the N- and M-domains and include the N-terminal loop closing over the ATP binding site, the N-terminal helix that performs a swapping reaction with the N-domain in the neighboring subunit as well as the N-M interface, comprising the catalytic loop.

*ATP hydrolysis rate does not reflect functionality*

Our analysis shows that the ATP hydrolysis rate *per se* is not a good predictive indicator for Hsp90 functionality. The most striking examples are the Δ8 and the E33A variants of Hsp90. Δ8 Hsp90 exhibits a two-fold increase in ATP turnover rate relative to the wildtype protein and should thus be a good substitute for wildtype Hsp90. However, this mutant is completely defective *in vivo*. Our mechanistic analysis revealed that Δ8 Hsp90 does not adopt the open conformation as effectively as the wildtype protein. Rather, as shown by SAXS and FRET, it exhibits a compact, N-terminally associated form even in the absence of nucleotide. In contrast, the E33A variant does not hydrolyze ATP at detectable rate, while supporting growth. This is consistent with the differences in chemical shifts in $^{1}H,^{15}N$-HSQC NMR spectra between the mutant Δ8 and the wildtype protein that spread over the whole N-terminal domain, suggesting a different conformational state of the N-terminal domain in the absence of nucleotide. These findings imply that the speed of the cycle plays a subordinate role. Instead the conformations that are adopted along the way and the time Hsp90 spends in a specific conformational state are critical. Thus, the cycling between conformational states has tremendous consequences on the biological function.

In this respect the mutants used in this study reveal four different categories of variations of the ATPase cycle (**Fig. 8**): 1) mutations that dramatically affect the hydrolysis properties, but allow the initial conformational changes to occur almost normal, like E33A (**Fig. 8b**). These mutations apparently do not affect functionality to an extent that precludes growth, but renders yeast stress-sensitive 2) mutations that decelerate the transition between the closed-1 and closed-2 states, such as R380A), thereby accumulating the closed-1 state under equilibrium cycling conditions(**Fig. 8c**. 3) mutations that alter the closing rate of the

chaperone, while still supporting growth. R346S (**Fig. 8c**) in particular affects the initial conformational changes dramatically. Some of these differences apparently can be altered by cofactors, leading to a "repair" of the defects. 4) mutants that accumulate closed states during normal cycle progression on the expense of cycle progression. This is true for Δ8-Hsp90 (**Fig. 8d**), which hydrolyses at almost normal speed, but shows strongly altered populations of conformational states. Here apparently the timing of different states within the cycle is decisive for the *in vivo* functionality and thus renders Δ8-Hsp90 dysfunctional.

Where do the dramatical differences between these mutants originate from, in particular as many of them reside in the N-terminal domain? The analysis of two residues in the ATP binding pocket, E33A and D79N, directly implicated in ATP hydrolysis or binding[13,14], respectively, revealed further unexpected results on the importance of ATP binding and hydrolysis on Hsp90 function. Differences in chemical shifts between E33A and the wildtype protein are distributed over the whole N-terminal domain, consistent with an important effect on domain conformation. D79N does not bind ATP and accordingly does not undergo any conformational changes in response to nucleotide. E33A, on the other hand, binds ATP and our analysis shows that it responds to ATP binding with changes in conformation and specifically with the accumulation of the closed-2 state. In contrast to previous results, the E33A variant conveyed viability to yeast in our experiments. However, the yeast strain exhibited increased sensitivity to stress and defects in client interaction were detected both *in vivo* and *in vitro*. This variant seems to pass through the early intermediates like the wildtype protein but stops at the completely closed state. Inspection of the Hsp90 crystal structure shows that E33, R380, and the γ-phosphate of ATP are close in space. We speculate that E33 destabilizes the closed conformation and is important for efficient release of the hydrolyzed nucleotide. The closed state is more stable in the E33A mutant due to the absence of charge clashes with the γ-phosphate and the lack of destabilizing effects of the R380-γ-phosphate interaction. Thus, ATP binding is sufficient to support the first conformational transitions.

*Accumulation of the closed-2 state reduces Hsp90 functionality in vivo and client binding in vitro*

The analysis of mutants in different structural elements allows to draw general conclusions which go beyond explaining the contributions of a specific site to the mechanism of Hsp90. We find that mutations affecting the timing of the conformational transitions strongly impair the biological function of Hsp90 irrespective of their position.

In particular the effects observed with the mutants T22I, E33A and Δ8 Hsp90 allow correlating conformational changes to client processing and *in vivo* functionality. All three mutants accumulate the closed-2 state in contrast to the normal predominance of the open

conformation in the presence of ATP[17,20]. This suggests that the three mutants exhibit a different timing of the cycle and also different effects of conformational change on the processing of client proteins. In agreement with this notion, they bind GR with strikingly reduced affinity in the presence of ATP, implying that they accumulate the wrong conformation for client interaction. This is most evident for Δ8 Hsp90, which apparently accumulates the right conformation for high affinity GR-binding in the absence of ATP, but in presence of ATP the predominant conformation changes to the closed-2 state, which is less favorable for client interaction, leading to less bound GR in the complex[24].

For all three mutants *in vivo* functionality and client binding is reduced. The picture that emerges is that high affinity client binding requires a conformation with closed N-terminal domains, like Δ8 Hsp90 in the absence of ATP. Client is released, at least partially, if the closed-2 state is adopted. This is in accordance with results obtained for the interaction of the GR-LBD with Hsp90 where the use of non-hydrolysable nucleotides reduced GR-binding[24]. Thus, even if ATP turnover is possible, the functionality of Hsp90 can be compromised to an extent that excludes *in vivo* function, depending on which conformations are populated during cycling conditions.

*Co-chaperones can correct variants compromised in cycling.*

Co-chaperones play a decisive role in modulating the Hsp90 machinery. A striking example is the effect of Aha1 on the mutant R346S: it turns an ATPase-defective variant into a wildtype-like protein concerning cycle progression. Furthermore, these results demonstrate that co-chaperones target specific conformational intermediates. Aha1 shows effects exclusively on mutants with defects in the transition from the open to the N-terminally closed state consistent with its function in promoting N-terminal closure[22]. Comparison of the mutants R380A and R346S provides further clues about important features of the conformational cycle and Aha1 function. R380 is located in the so-called catalytic loop of the M-domain, a structural element which contacts the ATP binding site in the N-domain, while R346 is part of the N-M interface formed upon nucleotide binding. Both mutants lead to an almost identical reduction of the ATPase to about 1/3 of wildtype activity. Similarly, both mutants show deficiencies in adopting a closed conformation in the presence of ATPγS. If ATP turnover would be the critical determinant for Hsp90 function, then these mutants should behave similarly. However, the mutants show opposite *in vivo* effects. While the R380A substitution is lethal, R346S supports viability. Furthermore for R346S, client processing *in vivo* and client interaction *in vitro* are not affected. So what is the critical difference between the two mutants? Part of the puzzle was revealed when we discovered remarkable differences in the stimulation of their ATPase activities by the accelerator Aha1: while for R380A addition of Aha1 only doubled the ATP hydrolysis rate, R346S was stimulated almost

80-fold reaching a maximum velocity similar to the wildtype protein. The dissection of conformational states revealed that R346S has difficulties in the transition to closed-1, consistent with the enormous stimulation of the ATPase by Aha1. In contrast, for R380A this step is unaffected but the subsequent formation of the fully closed state (closed-2) is compromised, leading to the accumulation of closed-1. Evidence for this conclusion comes from the inability of this mutant to bind the co-chaperone p23, which is a sensor for the fully closed state[26]. Thus, although both N-M interface mutants slow down the closing reaction, the precise point at which the defect occurs plays a decisive role. Based on the crystal structure of Hsp90[16], R380 had been proposed to be a catalytic residue that contacts the γ-phosphate of ATP during the hydrolysis reaction. While the implication in catalysis is certainly suggestive, our data and results from the Agard lab[23] argue for an important contribution of this residue to the conformational transitions. The mutant can adopt the fully closed state and progress through the cycle, but does so with decreased efficiency. If hydrolysis is slowed down roughly by a factor of 10 in the presence of ATPγS, then the mutant behaves like wildtype; when hydrolysis is faster, then the defects in reaching the closed state become apparent. In this context, it should be noted that the adjacent residue S379 is targeted by phosphorylation leading to changes in the Hsp90 conformational cycles[34]. Thus, a high sensitivity of the catalytic loop for even small structural perturbations allows switching the function of the entire protein by modulating the conformational transitions.
In conclusion, the timing of the cycle, i.e. the time Hsp90 spends in a certain conformation is decisive for the interaction with client proteins and thus for the *in vivo* function of this molecular chaperone, irrespective of the overall cycle speed.

## Material and Methods

*Cloning and protein purification*

All Hsp90 point mutants were generated using Quick-Change (Stratagene, La Jolla, USA) site directed mutagenesis with pET28a containing wildtype yeast Hsp90 as template vector. The proteins were expressed in the *Escherichia coli* strain BL21 (DE3) RIL (Stratagene, La Jolla, USA) and the proteins were purified as described previously[34] and stored in 40 mM Hepes pH 7.5, 150 mM KCl 5 mM $MgCl_2$ (standard buffer) at -70°C until usage. Hsp90 co-chaperones were purified as described previously[35].

*Protein labeling*

Labeling of the Hsp90 cysteine variants was performed as described previously[17]. Sba1 was labeled via an engineered cysteine at position 2 with 5-iodacetamido-fluorescein (Invitrogen, Karlsruhe, Germany) according to manufacturer´s protocol. Free label was separated as previously described[25].

*ATPase activity*

ATPase assays were performed as described previously, using an ATP-regenerating system[36]. Assays were measured with a Hsp90 concentration of 3 µM in standard buffer supplemented with 2 mM ATP (Roche, Mannheim, Germany) at 30 °C. The Hsp90-specific ATPase activity was inhibited by adding 50 µM of the inhibitor radicicol (Sigma, St. Louis, USA). In the case of remaining activity, it was subtracted as background. The assays were evaluated using the Origin software (OriginLab Corporation, Northhampton, USA). The stimulation of ATPase activity was measured under comparable conditions except using 1 µM of Hsp90 in the presence of 40 µM Aha1.

*Nucleotide binding kinetics*

To analyze the conformational rearrangements after nucleotide binding, Hsp90 heterodimers (400 nM) were formed by mixing an equal amount of donor-labeled and acceptor-labeled Hsp90 in standard buffer. The experiment was started by addition of 2 mM nucleotide (ATP, ATP$\gamma$S, AMP-PNP all supplied by Roche, Mannheim, Germany) and the increase of fluorescence intensity was recorded using a Fluoromax 3 or Fluoromax 2 fluorescence spectrophotometer (Horiba Jobin Yvon, München, Germany) at 575 nm after excitement at 490 nm at 30 °C. The apparent rate constants of the conformational changes were determined by fitting the data to monoexponential function using the Origin software (OriginLab Corporation, Northhampton, USA).

*Subunit exchanges*

After heterodimer formation, the subunit exchange was recorded by addition of a 10-fold excess of unlabeled Hsp90 and the decay of fluorescence intensity was recorded using a

Fluoromax 3 or Fluoromax 2 fluorescence spectrophotometer (Horiba Jobin Yvon, München, Germany) at 575 nm after excitement at 490 nm at 30 °C. For experiments in the presence of different nucleotides (ATP, ATPγS, AMP-PNP all supplied by Roche, Mannheim, Germany), Hsp90 variants were preequilibrated 30 min in presence of 2 mM the respective nucleotide to allow the formation of the closed state. For chase-reactions in presence of p23, 5 µM was added to the preformed complex. The apparent half-life of the reaction was determined by fitting the data using the function for exponential decay with Origin software (OriginLab Corporation, Northhampton, USA).

*Analytical Ultracentrifugation*

To analyze the binding of Fluorescein-Sba1, and Atto 488-GR to Hsp90, analytical ultracentrifugation was performed in a Beckman ProteomeLab XL-A (Beckman, Krefeld, Germany) equipped with a fluorescence-detection system (Aviv Biomedica, Lakewood, USA). Sedimentation-velocity experiments were performed with labeled protein supplemented with various combinations of unlabeled proteins in standard buffer at 42,000 rpm. A Ti-50 Rotor (Beckman) was used at 20 °C. To determine the size of complexes, the raw data were converted to *dc/dt* profiles by subtracting nearby scans and converting the difference into *dc/dt* plots as described[37]. The plots generally correlated with those from the SEDVIEW dc/dt program[38]. *dc/dt* profiles were analyzed by using bi-Gaussian functions to determine the *s*-values and the areas of the corresponding peaks.

*NMR Spectroscopy*

All spectra were recorded on a Bruker AVIII 600 MHz spectrometer with cryogenic triple resonance gradient probe. A construct comprising the first 210 residues of yeast Hsp90 was used to record $^{1}H,^{15}N$-HSQC spectra of the wildtype protein and the mutants Δ8, A10T, L18R, T22I, E33A, D79N, and A107N. Protein concentrations were in a range between 110 and 465 µM. In case of E33A and D79N in addition, $^{15}N$-edited NOESY spectra were recorded to confirm assignments of the mutants. All spectra were acquired in a 20 mM sodium phosphate buffer (pH 6.5) containing 100 mM sodium chloride, 2 mM EDTA, 1 mM DTT and 5% $D_2O$. The mutants E33A, D79N, and A107N were measured also in complex with a 2:1 excess of AMP-PNP. For these measurements 4 mM magnesium sulfate was added to the sample. All spectra were processed with NMRPipe/Draw[39] and analyzed with CcpNmr analysis[40]. The chemical shift perturbation (CSP) has been calculated according to the following formula, where δ is the proton (H) or nitrogen (N) chemical shift of the wildtype (wt) or mutant (mut).

$$CSP = \sqrt{(\delta_{Hwt} - \delta_{Hmut})^2 + \left(\frac{(\delta_{Nwt} - \delta_{Nmut})}{10}\right)^2}$$

*Small angle X-ray scattering*

SAXS data for solutions of the nucleotide-free, ATP-, and ATPγS bound forms of wildtype yeast Hsp90 and Hsp90 mutants were recorded on an in-house SAXS instrument (SAXSess mc2, Anton Paar, Graz, Austria) equipped with a Kratky camera, a sealed X-ray tube source and a two-dimensional Princeton Instruments PI•SCX:4300 (Roper Scientific) CCD detector. The scattering patterns were measured with a 60-min exposure time (360 frames, each 10 seconds) for several solute concentrations in the range from 0.8 to 3.3 mg/ml (**Fig. 4**). Radiation damage was excluded based on a comparison of individual frames of the 60-min exposures, where no changes were detected. A range of momentum transfer of $0.012 < s < 0.63$ Å-1 was covered ($s = 4\pi \sin(\theta)/\lambda$, where $2\theta$ is the scattering angle and $\lambda = 1.5$ Å is the X-ray wavelength).

All SAXS data were analyzed with the package ATSAS (version 2.5). The data were processed with the SAXSQuant software (version 3.9), and desmeared using the program GNOM[41]. The forward scattering, I(0), the radius of gyration, Rg, the maximum dimension, Dmax, and the inter-atomic distance distribution functions, (P(R)), were computed with the program GNOM[41]. The masses of the solutes were evaluated by comparison of the forward scattering intensity with that of a human serum albumin reference solution (molecular mass 69 kDa).

*In vivo function of Hsp90 variants*

The *in vivo* functionality of the different Hsp90 variants was tested using a plasmid shuffling approach based on the system described previously[29]. We used the ΔECU82α *Saccharomyces cerevisiae* strain (a derivative of W303) obtained from Susan Lindquist‟s lab[29]. This yeast strain is deficient for genomic hsp82 and hsc82 and contains a plasmid coding for hsp82 to rescue lethality. This plasmid carries an URA selection marker, which enables a selection for cells that had lost the wildtype Hsp82 plasmid in the medium supplemented with 5‟FOA. Hsp90 wildtype and the mutant-variants were constitutively expressed from a 2 micron high-copy number plasmid under the control of a constitutive glyceraldehyde-3-phosphate dehydrogenase gene (GPD) promotor (p423GPD vector). The cells surviving the shuffling were tested for loss of the URA-plasmid by plating out on respective selection media lacking URA.

*UV-damage repair assay, v-Src and GR maturation assay*

Experiments were performed as previously described[34].

1. Zhao, R. et al. Navigating the chaperone network: an integrative map of physical and genetic interactions mediated by the hsp90 chaperone. *Cell* **120**, 715-27 (2005).
2. Young, J.C., Moarefi, I. & Hartl, F.U. Hsp90: a specialized but essential protein-folding tool. *J Cell Biol* **154**, 267-73 (2001).
3. Richter, K., Haslbeck, M. & Buchner, J. The heat shock response: life on the verge of death. *Mol Cell* **40**, 253-66 (2010).
4. Picard, D. Heat-shock protein 90, a chaperone for folding and regulation. *Cell Mol Life Sci* **59**, 1640-8 (2002).
5. McClellan, A.J. et al. Diverse cellular functions of the Hsp90 molecular chaperone uncovered using systems approaches. *Cell* **131**, 121-35 (2007).
6. Taipale, M., Jarosz, D.F. & Lindquist, S. HSP90 at the hub of protein homeostasis: emerging mechanistic insights. *Nat Rev Mol Cell Biol* **11**, 515-28 (2010).
7. Prodromou, C. et al. Identification and structural characterization of the ATP/ADP-binding site in the Hsp90 molecular chaperone. *Cell* **90**, 65-75 (1997).
8. Nemoto, T., Ohara-Nemoto, Y., Ota, M., Takagi, T. & Yokoyama, K. Mechanism of dimer formation of the 90-kDa heat-shock protein. *Eur J Biochem* **233**, 1-8 (1995).
9. Bose, S., Weikl, T., Bugl, H. & Buchner, J. Chaperone function of Hsp90-associated proteins. *Science* **274**, 1715-7 (1996).
10. Wegele, H., Muschler, P., Bunck, M., Reinstein, J. & Buchner, J. Dissection of the contribution of individual domains to the ATPase mechanism of Hsp90. *J Biol Chem* **278**, 39303-10 (2003).
11. Prodromou, C. et al. The ATPase cycle of Hsp90 drives a molecular 'clamp' via transient dimerization of the N-terminal domains. *EMBO J* **19**, 4383-92 (2000).
12. Smith, D.F. Tetratricopeptide repeat cochaperones in steroid receptor complexes. *Cell Stress Chaperones* **9**, 109-21 (2004).
13. Panaretou, B. et al. ATP binding and hydrolysis are essential to the function of the Hsp90 molecular chaperone in vivo. *EMBO J* **17**, 4829-36 (1998).
14. Obermann, W.M., Sondermann, H., Russo, A.A., Pavletich, N.P. & Hartl, F.U. In vivo function of Hsp90 is dependent on ATP binding and ATP hydrolysis. *J Cell Biol* **143**, 901-10 (1998).
15. Shiau, A.K., Harris, S.F., Southworth, D.R. & Agard, D.A. Structural Analysis of E. coli hsp90 reveals dramatic nucleotide-dependent conformational rearrangements. *Cell* **127**, 329-40 (2006).
16. Ali, M.M. et al. Crystal structure of an Hsp90-nucleotide-p23/Sba1 closed chaperone complex. *Nature* **440**, 1013-7 (2006).
17. Hessling, M., Richter, K. & Buchner, J. Dissection of the ATP-induced conformational cycle of the molecular chaperone Hsp90. *Nat Struct Mol Biol* **16**, 287-93 (2009).
18. Weikl, T. et al. C-terminal regions of Hsp90 are important for trapping the nucleotide during the ATPase cycle. *J Mol Biol* **303**, 583-92 (2000).
19. Mickler, M., Hessling, M., Ratzke, C., Buchner, J. & Hugel, T. The large conformational changes of Hsp90 are only weakly coupled to ATP hydrolysis. *Nat Struct Mol Biol* **16**, 281-6 (2009).
20. Krukenberg, K.A., Forster, F., Rice, L.M., Sali, A. & Agard, D.A. Multiple conformations of E. coli Hsp90 in solution: insights into the conformational dynamics of Hsp90. *Structure* **16**, 755-65 (2008).
21. Koulov, A.V. et al. Biological and structural basis for Aha1 regulation of Hsp90 ATPase activity in maintaining proteostasis in the human disease cystic fibrosis. *Mol Biol Cell* **21**, 871-84 (2010).
22. Retzlaff, M. et al. Asymmetric activation of the hsp90 dimer by its cochaperone aha1. *Mol Cell* **37**, 344-54 (2010).
23. Cunningham, C.N., Southworth, D.R., Krukenberg, K.A. & Agard, D.A. The conserved arginine 380 of Hsp90 is not a catalytic residue, but stabilizes the closed conformation required for ATP hydrolysis. *Protein Sci* **21**, 1162-71 (2012).

24. Lorenz, O.R. et al. Modulation of the Hsp90 chaperone cycle by a stringent client protein. *Mol Cell* **53**, 941-53 (2014).
25. Li, J., Richter, K., Reinstein, J. & Buchner, J. Integration of the accelerator Aha1 in the Hsp90 co-chaperone cycle. *Nat Struct Mol Biol* **20**, 326-31 (2013).
26. Li, J., Richter, K. & Buchner, J. Mixed Hsp90-cochaperone complexes are important for the progression of the reaction cycle. *Nat Struct Mol Biol* **18**, 61-6 (2011).
27. Richter, K., Walter, S. & Buchner, J. The Co-chaperone Sba1 connects the ATPase reaction of Hsp90 to the progression of the chaperone cycle. *J Mol Biol* **342**, 1403-13 (2004).
28. Meyer, P. et al. Structural basis for recruitment of the ATPase activator Aha1 to the Hsp90 chaperone machinery. *EMBO J* **23**, 1402-10 (2004).
29. Nathan, D.F. & Lindquist, S. Mutational analysis of Hsp90 function: interactions with a steroid receptor and a protein kinase. *Mol Cell Biol* **15**, 3917-25 (1995).
30. Toogun, O.A., Dezwaan, D.C. & Freeman, B.C. The hsp90 molecular chaperone modulates multiple telomerase activities. *Mol Cell Biol* **28**, 457-67 (2008).
31. Echtenkamp, F.J. et al. Global functional map of the p23 molecular chaperone reveals an extensive cellular network. *Mol Cell* **43**, 229-41 (2011).
32. Mimnaugh, E.G., Worland, P.J., Whitesell, L. & Neckers, L.M. Possible role for serine/threonine phosphorylation in the regulation of the heteroprotein complex between the hsp90 stress protein and the pp60v-src tyrosine kinase. *J Biol Chem* **270**, 28654-9 (1995).
33. Xu, Y. & Lindquist, S. Heat-shock protein hsp90 governs the activity of pp60v-src kinase. *Proc Natl Acad Sci U S A* **90**, 7074-8 (1993).
34. Soroka, J. et al. Conformational switching of the molecular chaperone Hsp90 via regulated phosphorylation. *Mol Cell* **45**, 517-28 (2012).
35. Buchner, J., Weikl, T., Bugl, H., Pirkl, F. & Bose, S. Purification of Hsp90 partner proteins Hop/p60, p23, and FKBP52. *Methods Enzymol* **290**, 418-29 (1998).
36. Richter, K., Muschler, P., Hainzl, O. & Buchner, J. Coordinated ATP hydrolysis by the Hsp90 dimer. *J Biol Chem* **276**, 33689-96 (2001).
37. Stafford, W.F., 3rd. Boundary analysis in sedimentation transport experiments: a procedure for obtaining sedimentation coefficient distributions using the time derivative of the concentration profile. *Anal Biochem* **203**, 295-301 (1992).
38. Hayes, D.B. & Stafford, W.F. SEDVIEW, real-time sedimentation analysis. *Macromol Biosci* **10**, 731-5 (2010).
39. Delaglio, F. et al. NMRPipe: a multidimensional spectral processing system based on UNIX pipes. *J Biomol NMR* **6**, 277-93 (1995).
40. Vranken, W.F. et al. The CCPN data model for NMR spectroscopy: development of a software pipeline. *Proteins* **59**, 687-96 (2005).
41. Svergun, D.I. Determination of the regularization parameter in indirect-transform methods using perceptual criteria. *J Appl Cryst*, 495-503 (1992).
42. Richter, K., Reinstein, J. & Buchner, J. N-terminal residues regulate the catalytic efficiency of the Hsp90 ATPase cycle. *J Biol Chem* **277**, 44905-10 (2002).
43. Hubert, D.A., He, Y., McNulty, B.C., Tornero, P. & Dangl, J.L. Specific Arabidopsis HSP90.2 alleles recapitulate RAR1 cochaperone function in plant NB-LRR disease resistance protein regulation. *Proc Natl Acad Sci U S A* **106**, 9556-63 (2009).
44. Vaughan, C.K., Piper, P.W., Pearl, L.H. & Prodromou, C. A common conformationally coupled ATPase mechanism for yeast and human cytoplasmic HSP90s. *FEBS J* **276**, 199-209 (2009).
45. Meyer, P. et al. Structural and functional analysis of the middle segment of hsp90: implications for ATP hydrolysis and client protein and cochaperone interactions. *Mol Cell* **11**, 647-58 (2003).

**Acknowledgements**

We acknowledge C. Göbl and C. Hartlmüller for help with the SAXS measurements, Joanna Soroka and Jochen Reinstein for inspiring discussions and comments on the manuscript. F.T. acknowledges a scholarship from the Studienstiftung des deutschen Volkes. This work was supported by the Bavarian Ministry of Sciences, Research and the Arts (Bavarian Molecular Biosystems Research Network, to T.M.), the Austrian Academy of Sciences (APART-fellowship, to T.M.), the Deutsche Forschungsgemeinschaft (SFB1035 to J.B. and M.S; Emmy Noether program MA 5703/1-1, to T.M.).

**Figure legends**

**Figure 1: Localization and ATPase activities of selected yHsp90 mutants.** (**a**) Mutated residues are shown as red spheres in the crystal closed structure of yeast Hsp90 (pdb 2CG9) and the N-terminal domain in the open conformation (pdb 1AH6). The N-domain is highlighted in blue, the M-domain in green and the C-domain in orange and the lid structure is highlighted in cyan. (**b**) Influence of mutations on the ATPase activity of Hsp90. The coupled enzymatic ATPase assay was performed at 30°C in the presence of 2mM ATP. Error bars indicate SD (**c**) Stimulation of the by the cochaperone Aha1. Shown is the fold increase in ATPase activity of 1µM Hsp90 in the presence of 40 µM Aha1.

**Figure 2: NMR analysis of Mutants in the N-domain.** (**a**) Amide chemical shift differences larger than 0.03 ppm observed in 1H,15N-HSQC spectra of the Hsp90 N-domain mutants compared to the wildtype protein are indicated by red spheres on the crystal structure of the residues 1-210 of yeast Hsp90 (PDB: 1AM1). Residues with large chemical shift changes in the mutant cannot be unambiguously assigned and are indicated by salmon spheres, while residues which are not assigned in the wildtype protein are shown in grey. Bound ADP is shown in orange to indicate the nucleotide binding site. The position of the mutation is indicated by a green sphere. (**b**) Differences in chemical shift larger than 0.05 ppm between the free mutant and the complex with AMP-PNP are indicated as in (**a**). Residues that cannot be assigned in the complex are indicated by salmon spheres and unassigned residues in the free mutant in grey.

**Figure 3: N-terminal closing of the different Hsp90 variants.** Shown are the changes in acceptor fluorescence of the different Hsp90 variants in response to the binding of (**a**) 2mM ATPγS and (**b**) 2mM ATP. (**c**) Apparent half-lives ($t_{1/2}$) derived from a non-linear fit of the acceptor signal changes to mono-exponential functions of the disruption of 400 nM FRET-complex of the different Hsp90 variants by addition of 10-fold excess of the unlabeled Hsp90-variant in the absence of nucleotide (black) and in the presence of 2 mM ATP (red), 2 mM ATPγS (blue) or 2 mM AMP-PNP (dark cyan).

**Figure 4: SAXS analysis of yHsp90 variants.** P(R)-curves of wildtype and mutant Hsp90 in (**a**) the absence of nucleotide, in the presence of 4 mM (**b**) ATPγS or (**c**) ATP. Mutants for which significant differences in the P(R) were observed are shown in the right panel, mutants for which nor or only minor differences were observed are shown in the left panel.

**Figure 5: Binding of the co-chaperone Sba1/p23 to the Hsp90 variants.** The binding of 500 nM fluorescein-labeled Sba1/p23 to 1.5 µM Hap90 variant was analyzed by analytical ultracentrifugation with fluorescence detection in presence of (**a**) 2mM ATPγS and (**c**) 2mM

ATP. The areas of the complex peaks in presence of (**b**) 2mM ATPγS and (**d**) 2mM ATP were determined by fitting to bi-Gaussian function.

**Figure 6: Influence of Hsp90 variants on yeast growth and DNA repair.** (**a**) Viability of the Hsp90 variants. Δ8-, D79N, and R380A Hsp90-variants are not able to support yeast viability in contrast to wt, A10T-, L18R-, T22I-, A107N-, and R346S. (**b**) Yeast cells expressing different Hsp90 variants were adjusted to OD 0.5, serial dilutions were spotted and incubated at 24°C, 30°C or 37°C to test for temperature sensitivity. (**c**) To test for DNA repair activity of the Hsp90 variants, yeast cells were adjusted to OD 0.5 and exposed to different doses of UV light and incubated at 30°C.

**Figure 7: Influence of Hsp90 variants on client processing.** (**a**) Yeast cells expressing the different Hsp90 variants as only source of Hsp90 and v-Src under control of a galactose promoter were adjusted to OD 0.5 and spotted on glucose and galactose containing drop out plates and incubated at 30°C. (**b**) Influence of Hsp90 mutations on GR-processing in yeast cells. (**c**) Binding of the GR to different Hsp90 mutants detected by analytical ultracentrifugation with fluorescence detection: peak areas of GR-Hsp90 complex in presence of ATP (**d**) derived from dc/dt plots (**e**) and peak areas of GR-Hsp90 complex in absence of ATP (**f**) derived from dc/dt plots (**g**).

**Figure 8: Schematic representation of mutation-induced changes to the ATPase cycle.** The ATPase cycle is depicted as a scheme to illustrate the differences in turnover of different mutants. The dwelling time in different states for wildtype Hsp90 is based on Hessling *et al.*[17]. The changes in the Hsp90 mutants summarize the results from this study. The sectors indicate the relative time spent by the mutated protein in the different states during one round of hydrolysis. Other mutants which show less intense effects, like D107N, T22I, or which do not bind nucleotide, like D79N, are not depicted. The white sector in the scheme for E33A-Hsp90 indicates that hydrolysis does not detectably occur and therefore the mutant does not seem to pass beyond this state, as also reflected by the infinite number for the cycle time. The average cycle time of the other mutant proteins is given by the number in the center of the circle.

**Supplementary Figure 1: Thermal stability of yHsp90 variants**. Shown is the change of sypro-orange Fluorescence after excitation at 475 nm and emission at 590 nm with increasing temperature in the presence of 5 µg of the different yHsp90 variants. The measurements were performed in 40 mM Hepes/KOH pH 7.5, 150 mM KCl, and 5 mM $MgCl_2$.

**Supplementary Figure 2: Structural mapping of chemical shift perturbations for Hsp90 mutants.** (**a**) Amide chemical shift differences larger than 0.03 ppm observed in $^{1}H,^{15}N$-HSQC spectra of the Hsp90 N-domain mutants compared to the wildtype protein are indicated by red spheres in the crystal structure of residues 1-210 of yeast Hsp90 (PDB: 1AM1). Residues with large chemical shift changes in the mutant cannot be unambiguously assigned and are indicated by salmon spheres, while residues which are not assigned in the wildtype protein are shown in grey. Bound ADP is shown in orange to indicate the nucleotide binding site. The position of the mutation is indicated by a green sphere. (**b**) Blue spheres indicate residues involved in Aha1 binding.

**Supplementary Figure 3: $^{1}H,^{15}N$-HSQC spectra of the Hsp90 N-domain mutants**. $^{1}H,^{15}N$-HSQC spectra of the indicated mutant (red) are superposed with spectra of the wildtype (black) of the N-terminal domain of yeast Hsp90. Negative peaks are plotted in orange and grey respectively. Examples of strongly shifting peaks are zoomed.

**Supplementary Figure 4: Chemical shift perturbation plots of the Hsp90 N-domain mutants.** Chemical shift perturbation of the $^{1}H,^{15}N$-HSQC spectra from **Supplementary figure 3** between the indicated mutant and the wildtype of the N-terminal domain of yeast Hsp90. Negative chemical shifts indicate shifting residues that could not be assigned in the complex. Residues which are not assigned in the wildtype are indicated by gaps. Chemical shift changes larger than 0.15 ppm are indicated on top of the bars. The red lines at 0.03 ppm indicate the cutoff for chemical shifts marked in the plots on the structure.

**Supplementary Figure 5: $^{1}H,^{15}N$-HSQC spectra of the Hsp90 N-domain mutants in complex with AMP-PNP**. $^{1}H,^{15}N$-HSQC spectra of the indicated mutant of the N-terminal domain of yeast Hsp90 with (red) and without (black) AMP-PNP are superposed. Negative peaks are plotted in orange and grey respectively. Examples of strongly shifting peaks are zoomed.

**Supplementary Figure 6: Structural mapping of chemical shift perturbations for the E33A mutant.** Amide chemical shift differences larger than 0.05 ppm observed in $^{1}H,^{15}N$-HSQC spectra of the Hsp90 N-domain Mutant E33A between the free protein and the complex with AMP-PNP are indicated by red spheres on the crystal structure of residues 1-210 of yeast Hsp90 (PDB: 1AM1). Residues that cannot be assigned in the complex are indicated by salmon spheres and unassigned residues in the free mutant are plotted in grey. Bound ADP is shown in orange to indicate the nucleotide binding site. The position of the mutation is indicated by a green sphere.

**Tables**

**Table 1. Characteristics of analyzed Hsp90 variants.**

| variant | effect | literature |
|---|---|---|
| Δ8 | Increased closing in the presence of ATP | [42] |
| A10T | increased ATPase activity | [43] |
| L18R | decreased ATPase activity | [44] |
| T22I | *ts* mutant; increased ATPase activity | [11,29,44] |
| E33A | Hydrolysis deficient; lethality in yeast | [13,14] |
| D79N | loss of ATP binding and lethality in yeast | [13,14] |
| A107N | increased ATPase activity | [11,16] |
| R346S | decreased ATPase activity | [43] |
| R380A | decreased ATPase activity *in vitro* and lethality in yeast | [16,45] |

**Table 2. ATPase, Aha1 stimulation and rate constants of nucleotide-induced conformational changes of Hsp90 variants.**

| Hsp90 variant | ATPase activity | | | Aha1 stimulation | | | | Nucleotide-induced conformational changes | |
|---|---|---|---|---|---|---|---|---|---|
| | $k_{cat}$ ($min^{-1}$) | $K_M$ (mM) | $k_{cat}/K_M$ | $K_{Dapp}$ (µM) | $V_{max}$ ($min^{-1}$) | stimulation (x-fold) | $V_{max}/K_{Dapp}$ | $k_{app}$ (ATPγS) ($min^{-1}$) | $k_{app}$ (ATP) ($min^{-1}$) |
| wt | 0.55 ± 0.02 | 0.32 | 1.72 | 6.8 ± 0.7 | 12.9 ± 0.4 | 23 | 1.9 | 0.33 | - |
| Δ8 | 1.13 ± 0.05 | 0.07 | 16.14 | 1,3 ± 0.1 | 7.2 ± 0.1 | 6 | 5.5 | 1.05 | 1.53 |
| A10T | 0.84 ± 0.03 | 0.33 | 2.55 | 4.5 ± 0.6 | 17.4 ± 0.6 | 21 | 3.8 | 0.46 | - |
| L18R | 0.85 ± 0.06 | 0.77 | 1.10 | 3.3 ± 0.3 | 10.6 ± 0.2 | 12 | 3.2 | 0.30 | - |
| T22I | 0.85 ± 0.08 | 0.14 | 6.07 | 5.3 ± 0.9 | 5.1 ± 0.2 | 6 | 1.0 | 1.14 | 1.59 |
| E33A | < 0.001 | - | - | - | < 0.001 | 0 | - | 0.41 | 0.23 |
| D79N | < 0.001 | - | - | - | < 0.001 | 0 | - | - | - |
| A107N | 2.14 ± 0.08 | 0.01 | 21.40 | 3.7 ± 0.4 | 23.1 ± 0.4 | 11 | 6.2 | 0.72 | - |
| R346S | 0.17 ± 0.02 | 0.20 | 0.85 | 7.0 ± 1 | 13.4 ± 0.3 | 79 | 1.9 | 0.13 | - |
| R380A | 0.18 ± 0.06 | 0.36 | 0.50 | 2.1 ± 0.7 | 0.36 ± 0.02 | 2 | 0.2 | 0.15 | 0.20 |

ATPase activities were measured with a regenerative ATPase system at 30°C. Standard deviations were calculated from at least three measurements.

Nucleotide-induced conformational changes of the different Hsp90 variants were monitored by recording acceptor fluorescence after excitation of the donor. The increase in signal was fitted to a mono-exponential function to obtain the apparent rate constant. Dashes indicate no detectable conformational change

**Table 3. Apparent half-lives ($t_{1/2}$) of FRET-complexes of the Hsp90 variants in the presence of different nucleotides.**

| Hsp90 variant | $t_{1/2}$ (min) w/o nucleotide | $t_{1/2}$ (min) ATPγS | $t_{1/2}$ (min) AMP-PNP | $t_{1/2}$ (min) ATP | $t_{1/2}$ (min) ATP/p23 |
|---|---|---|---|---|---|
| wt | 0.5 | 49 | >300 | 0.9 | 0.8 |
| Δ8 | 1.0 | 60 | 2 | 8 | nd |
| A10T | 0.6 | 29 | 132 | 1 | nd |
| L18R | 0.5 | 13 | 3 | 0.8 | nd |
| T22I | 0.2 | 154 | 9 | 3 | nd |
| E33A | 0.6 | 12 | 0,4 | 30 | 107 |
| D79N | 0.7 | 1 | 1 | 0.7 | nd |
| A107N | 0.8 | 62 | >300 | 3 | nd |
| R346S | 0.5 | 28 | >300 | 0.4 | nd |
| R380A | 0.6 | 40 | 0.6 | 20 | 8 |

Shown are the half-lives of the FRET-complexes in absence and presence of 2 mM of different nucleotides after addition of tenfold excess of unlabeled Hsp90 variant. The half-lives were derived from fitting to mono-exponential functions to the decrease of acceptor signal during the reaction.

**Table 4. SAXS data and analysis.**

| Sample | $R_g$ [Å] | $D_{max}$ [Å] | Molecular mass [kDa]* |
|---|---|---|---|
| Hsp90 | 64.2 ± 0.2 | 240 | 173 |
| Δ8 | 61.9 ± 0.4 | 240 | 164 |
| L18R | 65.4 ± 0.6 | 240 | 181 |
| T22I | 69.3 ± 0.5 | 240 | 186 |
| E33A | 64.3 ± 0.7 | 260 | 171 |
| A107N | 68.0 ± 0.4 | 220 | 165 |
| R346S | 70.1 ± 0.2 | 240 | 162 |
| R380A | 68.7 ± 0.2 | 240 | 184 |
| Hsp90-ATP | 58.3 ± 0.1 | 220 | 185 |
| Δ8-ATP | 61.2 ± 0.1 | 220 | 164 |
| L18R-ATP | 66.5 ± 0.2 | 220 | 170 |
| T22I-ATP | 55.9 ± 0.2 | 220 | 180 |
| E33A-ATP | 58.7 ± 0.1 | 220 | 176 |
| A107N-ATP | 54.5 ± 0.4 | 220 | 167 |
| R346S-ATP | 65.3 ± 0.2 | 220 | 175 |
| R380A-ATP | 62.6 ± 0.1 | 220 | 179 |
| Hsp90-ATPγS | 53.5 ± 0.2 | 170 | 181 |
| Δ8- ATPγS | 55.6 ± 0.2 | 190 | 164 |
| L18R- ATPγS | 64.4 ± 0.1 | 220 | 167 |
| T22I- ATPγS | 52.0 ± 0.4 | 180 | 170 |
| E33A- ATPγS | 53.8 ± 0.2 | 180 | 162 |
| A107N- ATPγS | 55.1 ± 0.4 | 180 | 167 |
| R346S- ATPγS | 63.1 ± 0.2 | 220 | 184 |
| R380A- ATPγS | 61.1 ± 0.2 | 220 | 183 |

*The molecular mass was determined using Porod‟s law.

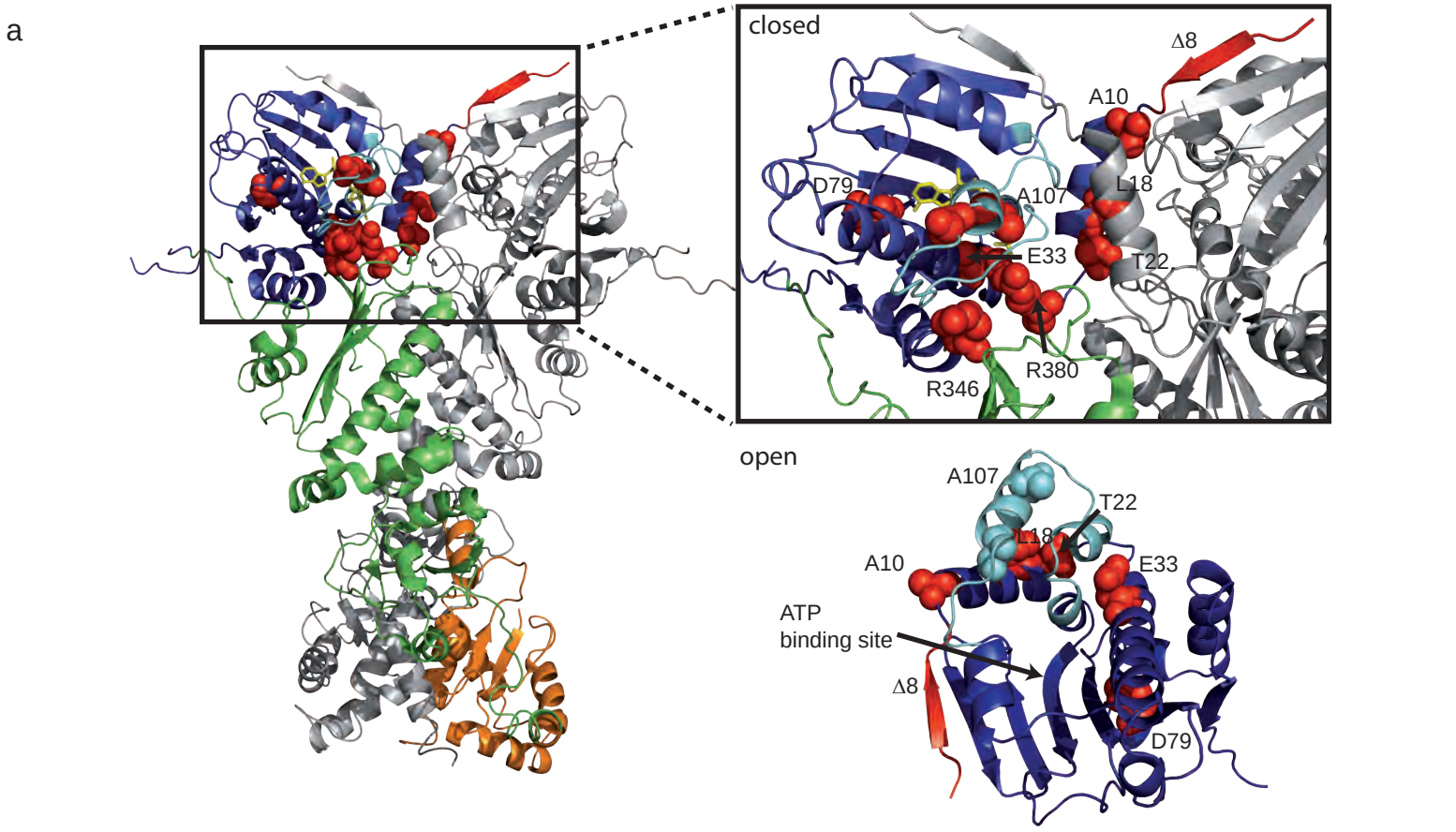
a
closed
Δ8
A10
D79
A107
L18
E33
T22
R380
R346
open
A107
T22
L18
A10
E33
ATP
binding site
Δ8
D79

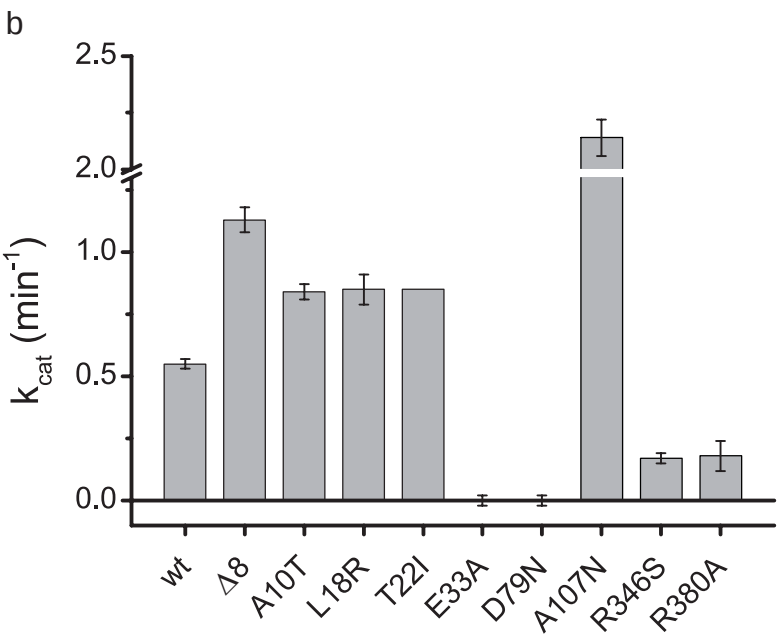
b
2.5
2.0
1.0
0.5
0.0
$k_{cat}$ ($min^{-1}$)
wt
Δ8
A10T
L18R
T22I
E33A
D79N
A107N
R346S
R380A

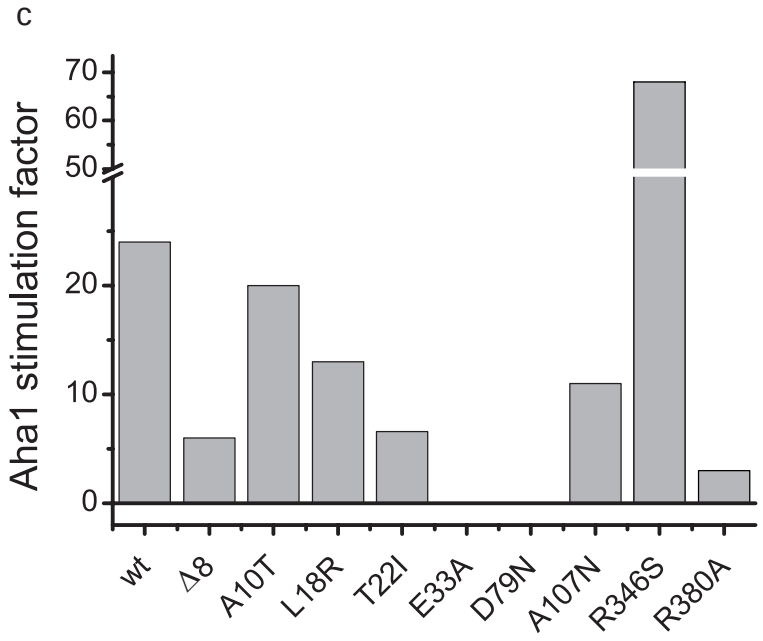
c
70
60
50
20
10
0
Aha1 stimulation factor
wt
Δ8
A10T
L18R
T22I
E33A
D79N
A107N
R346S
R380A

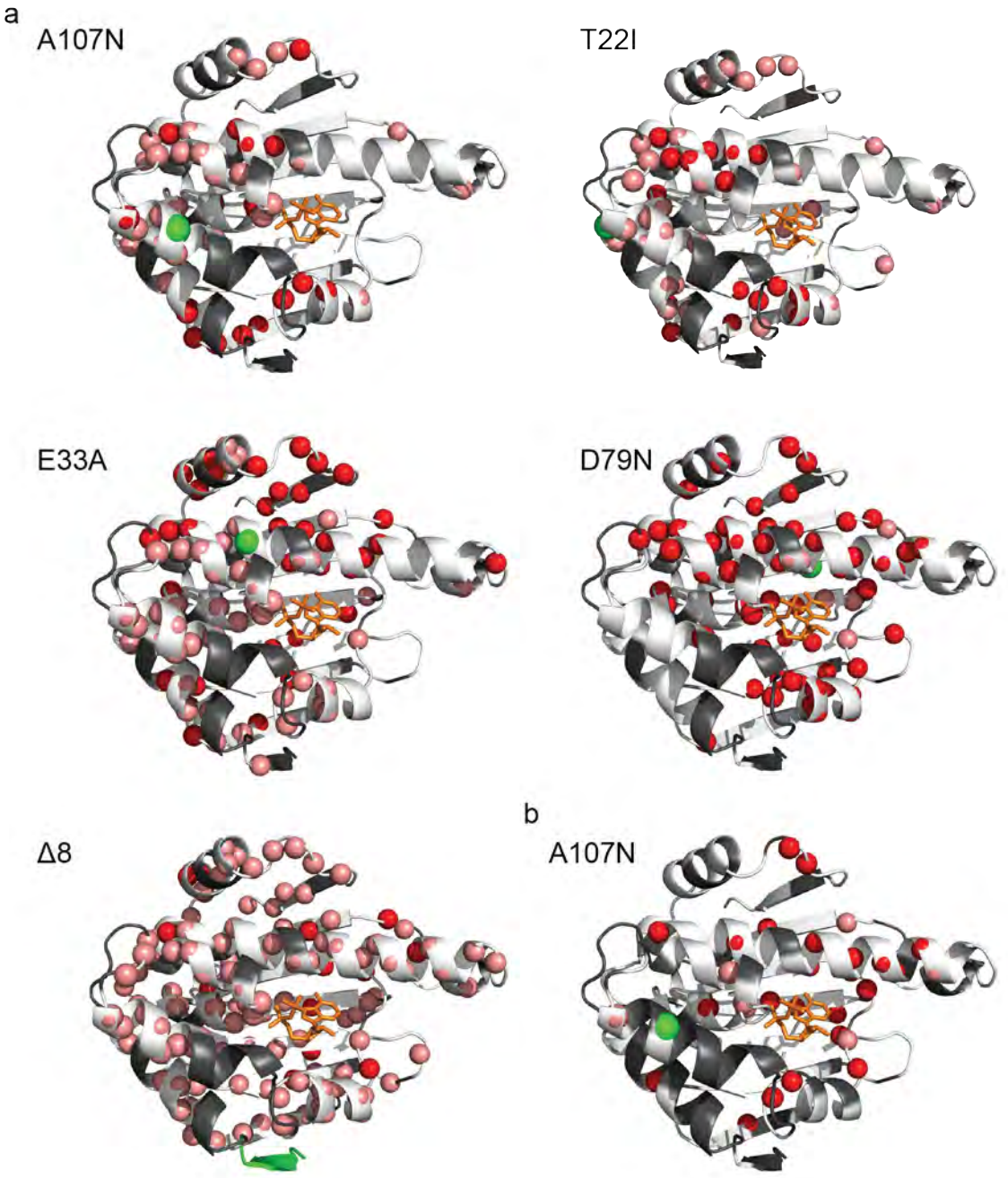
a
A107N
T22I
E33A
D79N
b
Δ8
A107N

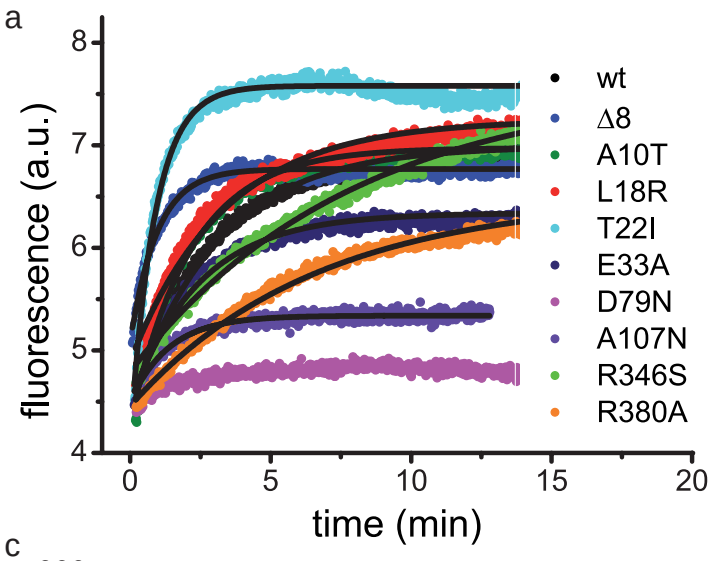
a
fluorescence (a.u.)
time (min)
wt
Δ8
A10T
L18R
T22I
E33A
D79N
A107N
R346S
R380A

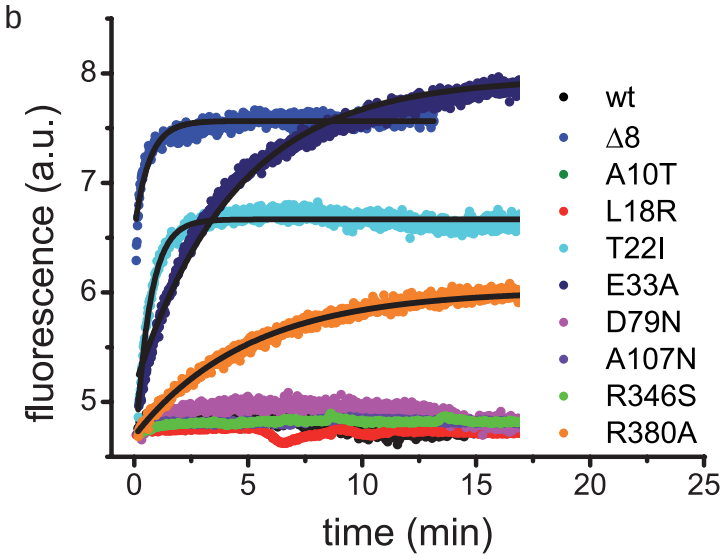
b
fluorescence (a.u.)
time (min)
wt
Δ8
A10T
L18R
T22I
E33A
D79N
A107N
R346S
R380A

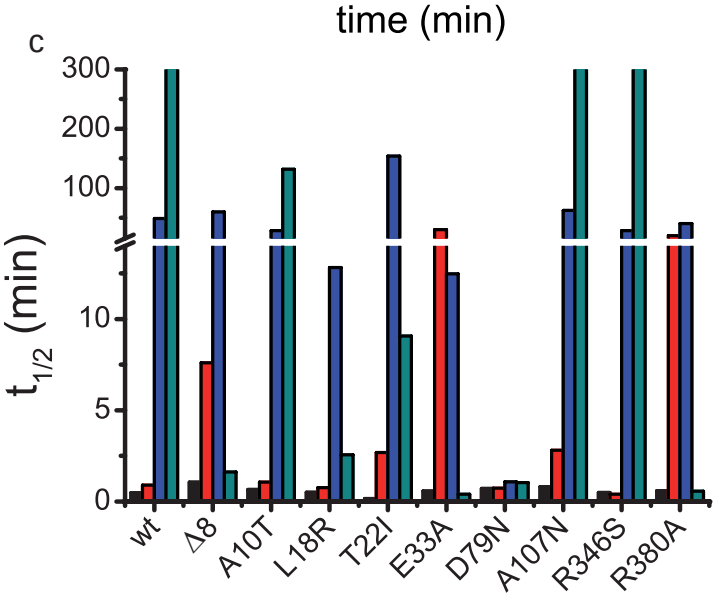
c
t1/2 (min)
wt
Δ8
A10T
L18R
T22I
E33A
D79N
A107N
R346S
R380A

a

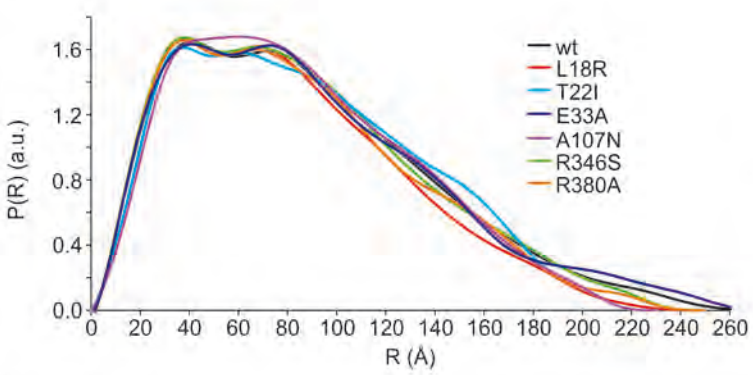
wt
L18R
T22I
E33A
A107N
R346S
R380A
P(R) (a.u.)
R (Å)

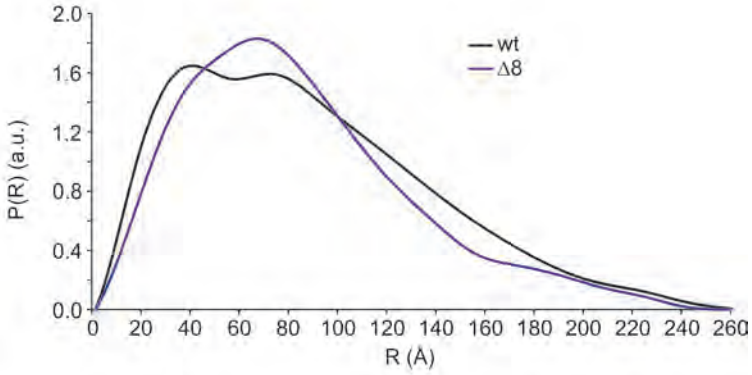
wt
Δ8
P(R) (a.u.)
R (Å)

b

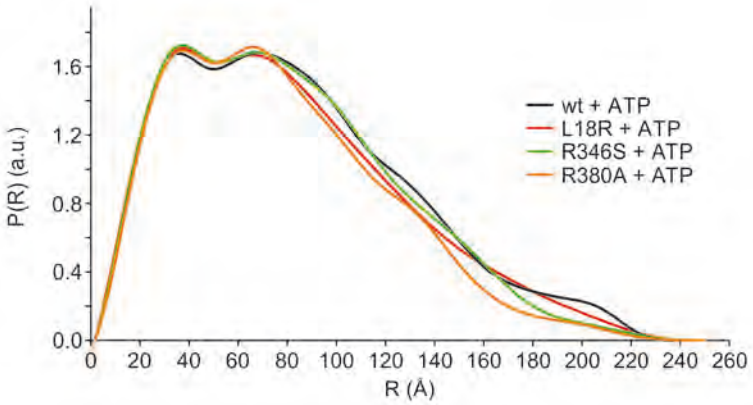
wt + ATP
L18R + ATP
R346S + ATP
R380A + ATP
P(R) (a.u.)
R (Å)

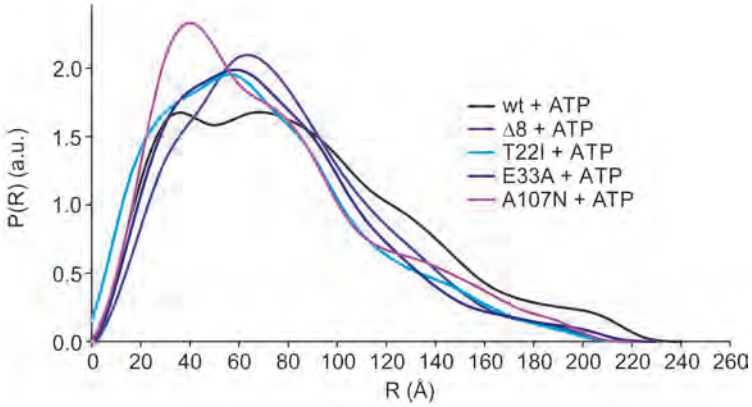
wt + ATP
Δ8 + ATP
T22I + ATP
E33A + ATP
A107N + ATP
P(R) (a.u.)
R (Å)

c

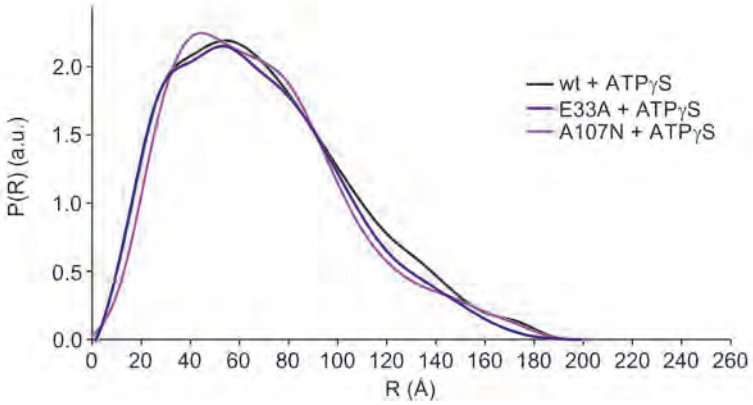
wt + ATPγS
E33A + ATPγS
A107N + ATPγS
P(R) (a.u.)
R (Å)

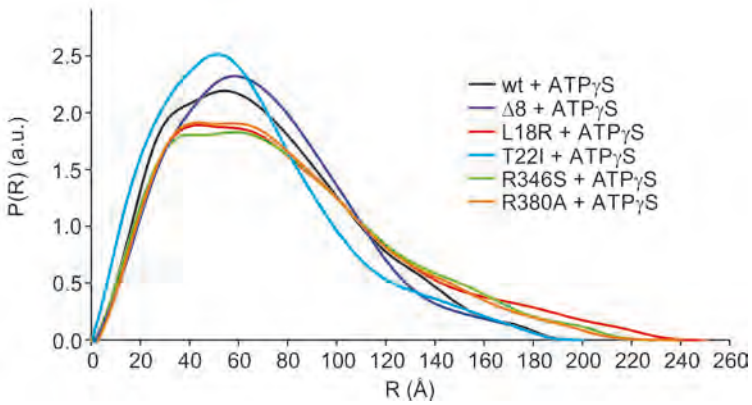
wt + ATPγS
Δ8 + ATPγS
L18R + ATPγS
T22I + ATPγS
R346S + ATPγS
R380A + ATPγS
P(R) (a.u.)
R (Å)

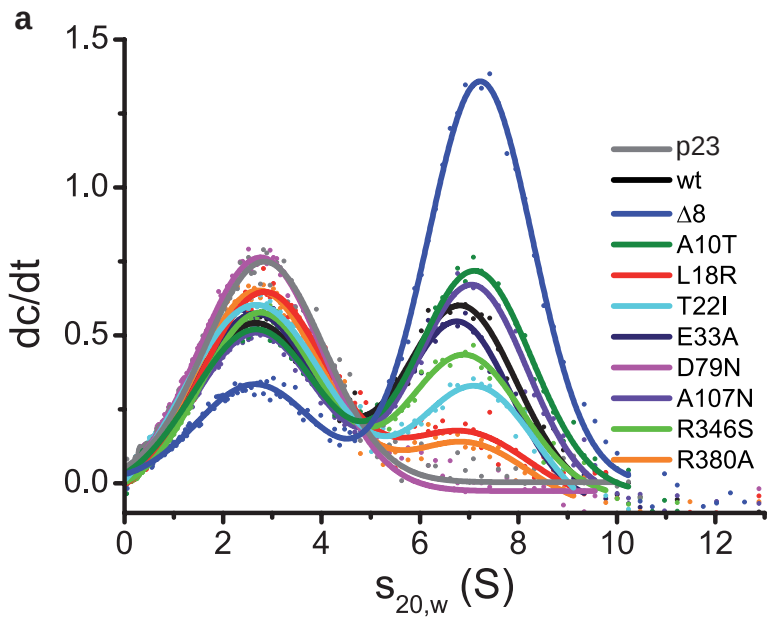
a
dc/dt
1.5
1.0
0.5
0.0
0
2
4
6
8
10
12
$s_{20,w}$ (S)
p23
wt
Δ8
A10T
L18R
T22I
E33A
D79N
A107N
R346S
R380A

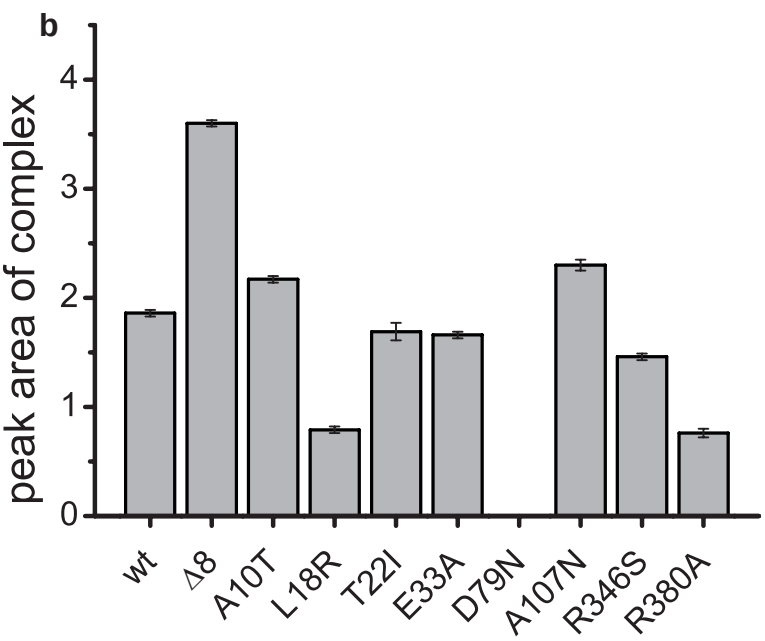
b
peak area of complex
4
3
2
1
0
wt
Δ8
A10T
L18R
T22I
E33A
D79N
A107N
R346S
R380A

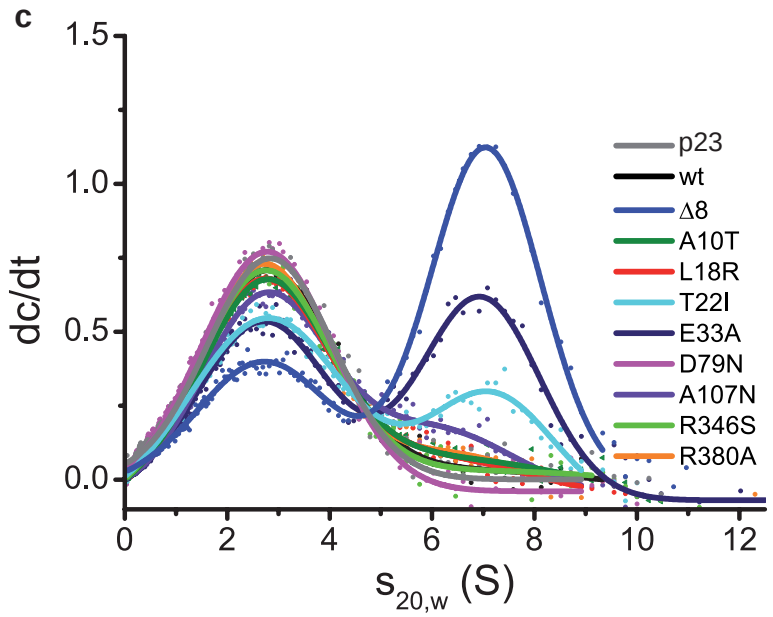
c
dc/dt
1.5
1.0
0.5
0.0
0
2
4
6
8
10
12
$s_{20,w}$ (S)
p23
wt
Δ8
A10T
L18R
T22I
E33A
D79N
A107N
R346S
R380A

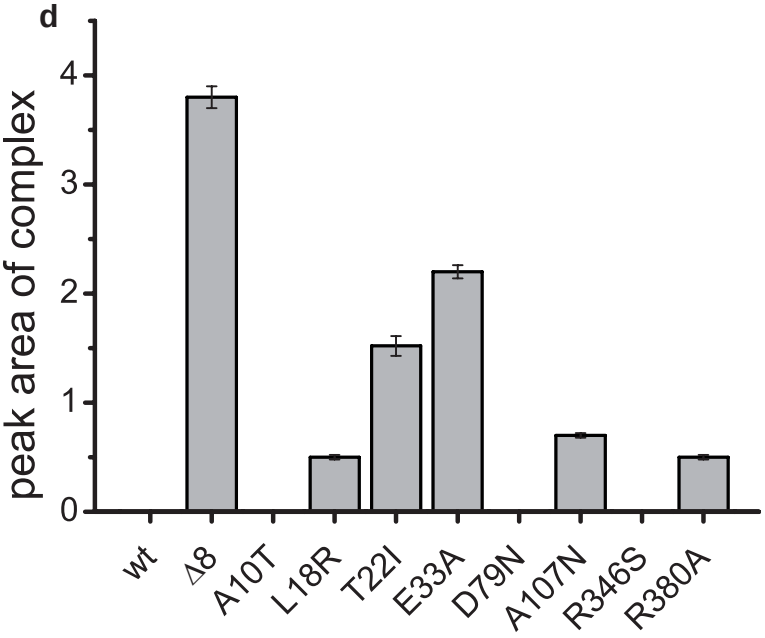
d
peak area of complex
4
3
2
1
0
wt
Δ8
A10T
L18R
T22I
E33A
D79N
A107N
R346S
R380A

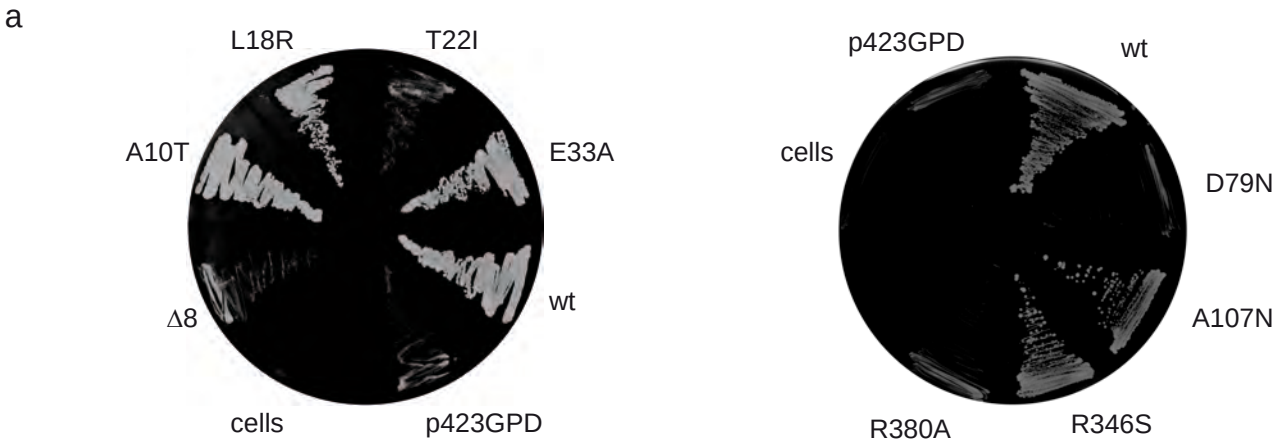
a
L18R
T22I
A10T
E33A
Δ8
wt
cells
p423GPD
p423GPD
wt
cells
D79N
A107N
R380A
R346S
b
24 °C
30 °C
37 °C
wt
A10T
L18R
T22I
E33A
A107N
R346S
c
0 J/m2
80 J/m2
120 J/m2
wt
A10T
L18R
T22I
E33A
A107N
R346S

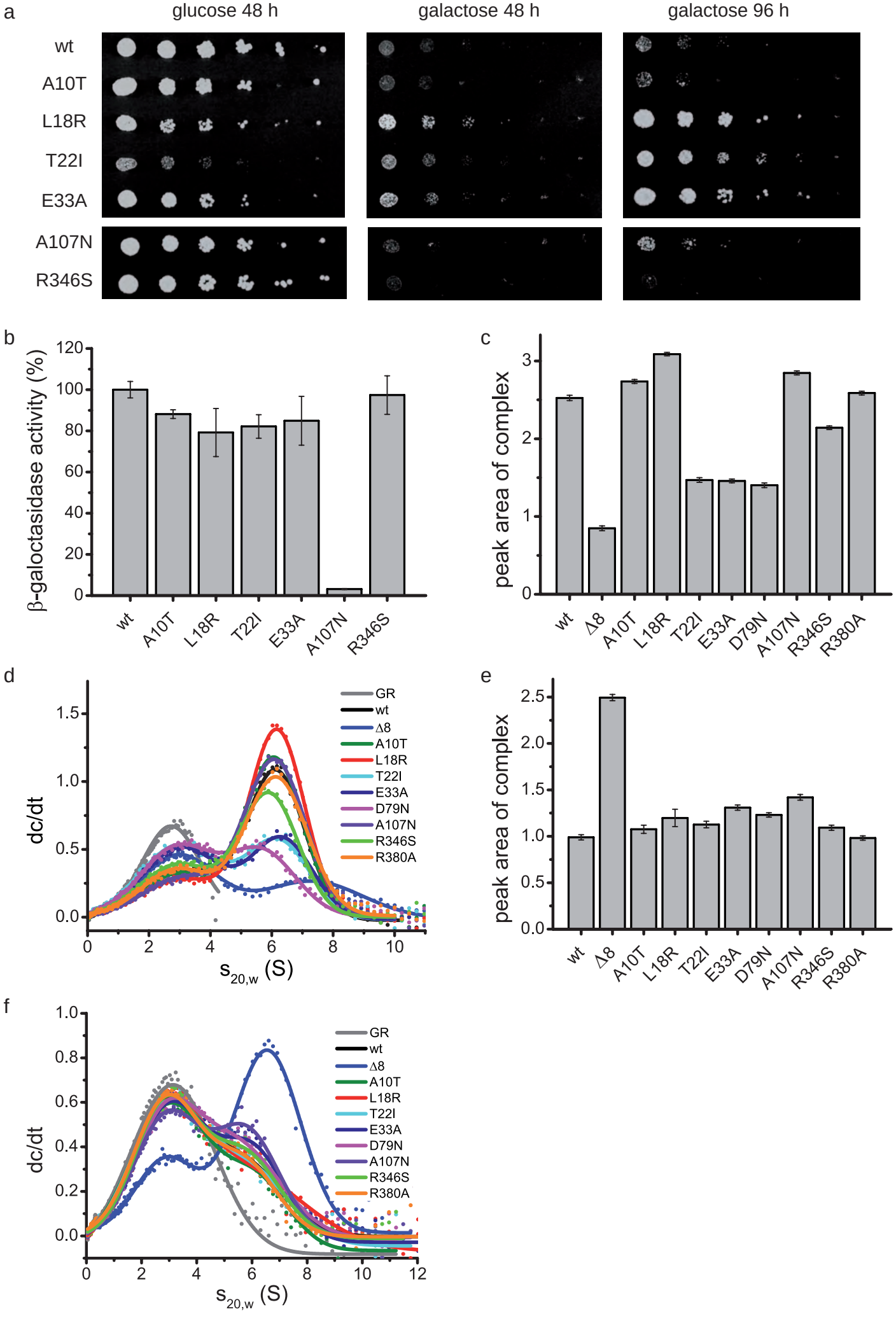
a
glucose 48 h
galactose 48 h
galactose 96 h
wt
A10T
L18R
T22I
E33A
A107N
R346S
b
β-galoctasidase activity (%)
0
20
40
60
80
100
120
wt
A10T
L18R
T22I
E33A
A107N
R346S
c
peak area of complex
0
1
2
3
wt
Δ8
A10T
L18R
T22I
E33A
D79N
A107N
R346S
R380A
d
dc/dt
0.0
0.5
1.0
1.5
0
2
4
6
8
10
s20,w (S)
GR
wt
Δ8
A10T
L18R
T22I
E33A
D79N
A107N
R346S
R380A
e
peak area of complex
0.0
0.5
1.0
1.5
2.0
2.5
wt
Δ8
A10T
L18R
T22I
E33A
D79N
A107N
R346S
R380A
f
dc/dt
0.0
0.2
0.4
0.6
0.8
1.0
0
2
4
6
8
10
12
s20,w (S)
GR
wt
Δ8
A10T
L18R
T22I
E33A
D79N
A107N
R346S
R380A

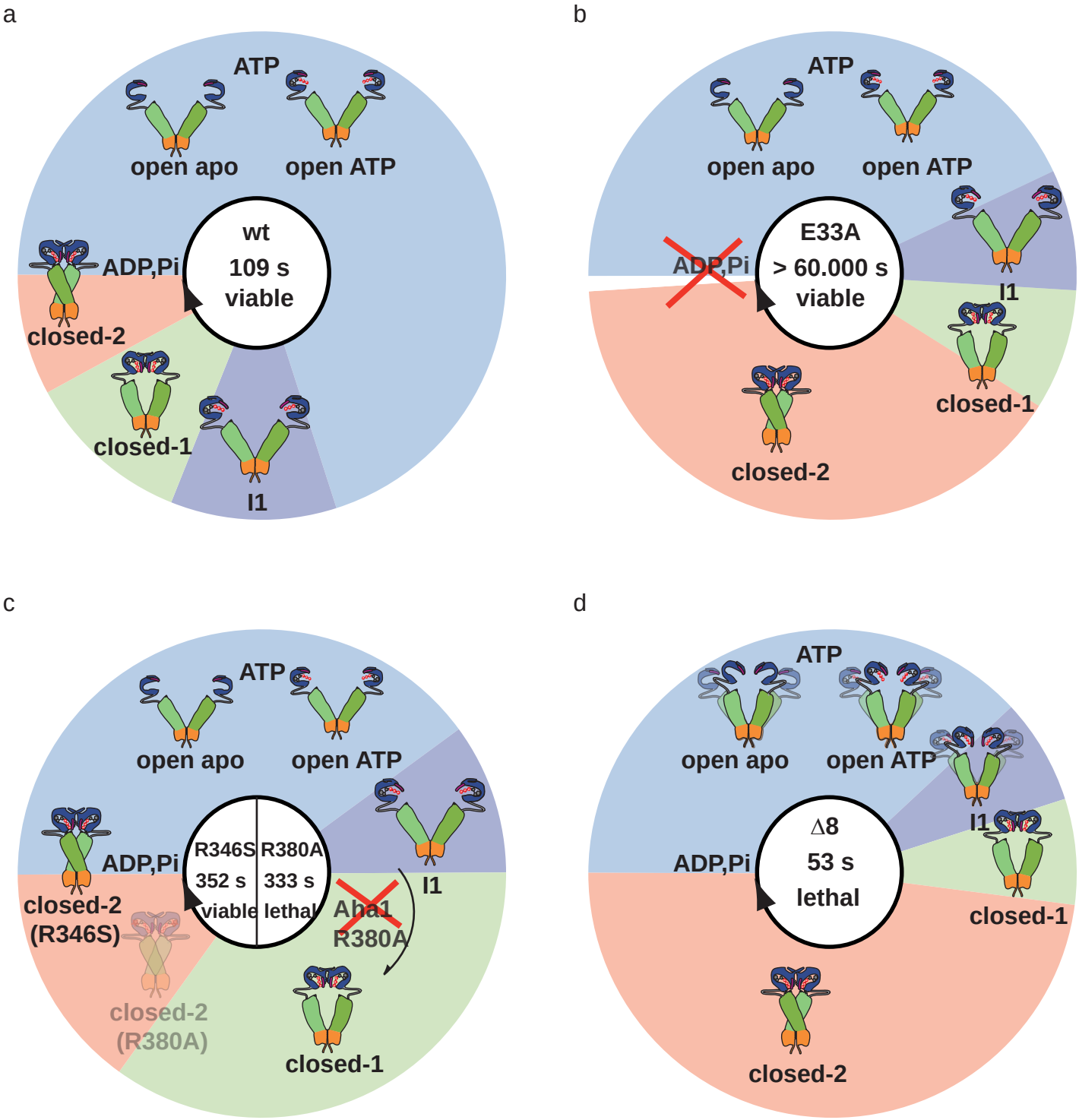
a
ATP
open apo
open ATP
wt
109 s
viable
ADP,Pi
closed-2
closed-1
I1
b
ATP
open apo
open ATP
E33A
> 60.000 s
viable
ADP,Pi
I1
closed-1
closed-2
c
ATP
open apo
open ATP
R346S
352 s
viable
R380A
333 s
lethal
ADP,Pi
I1
closed-2
(R346S)
Aha1
R380A
closed-2
(R380A)
closed-1
d
ATP
open apo
open ATP
Δ8
53 s
lethal
ADP,Pi
I1
closed-1
closed-2

# Importance of cycle timing for the function of the molecular chaperone Hsp90

Bettina K. Zierer [1)], Martin Rübbelke[1,2)], Tobias Madl[1,2,3)], Franziska Tippel[1)], Klaus Richter[1)], Michael Sattler[1,2)] and Johannes Buchner[1)]

1) Center for Integrated Protein Science Munich (CIPSM) at the Department of Chemistry Technische Universität München, Lichtenbergstr.4, 85747 Garching, Germany
2) Institute of Structural Biology, Helmholtz Zentrum München, 85764 Neuherberg, Germany
3) Institute of Molecular Biology & Biochemistry, Center of Molecular Medicine, Medical University of Graz, 8010 Graz, Austria

Supplementary Figure 1

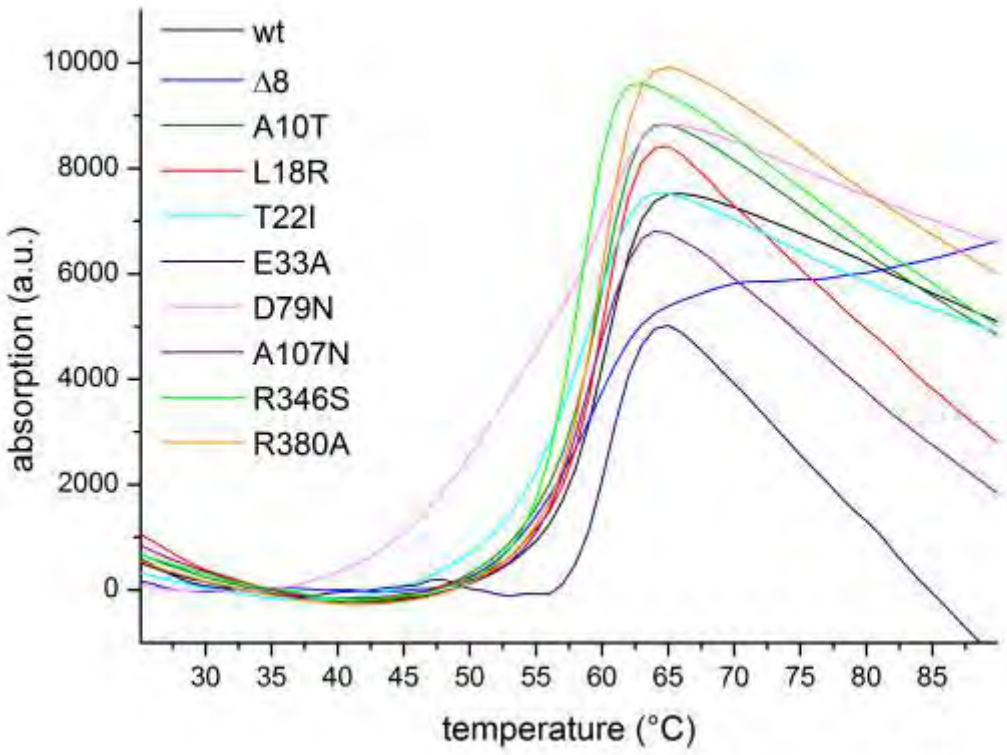

Supplementary Figure 2

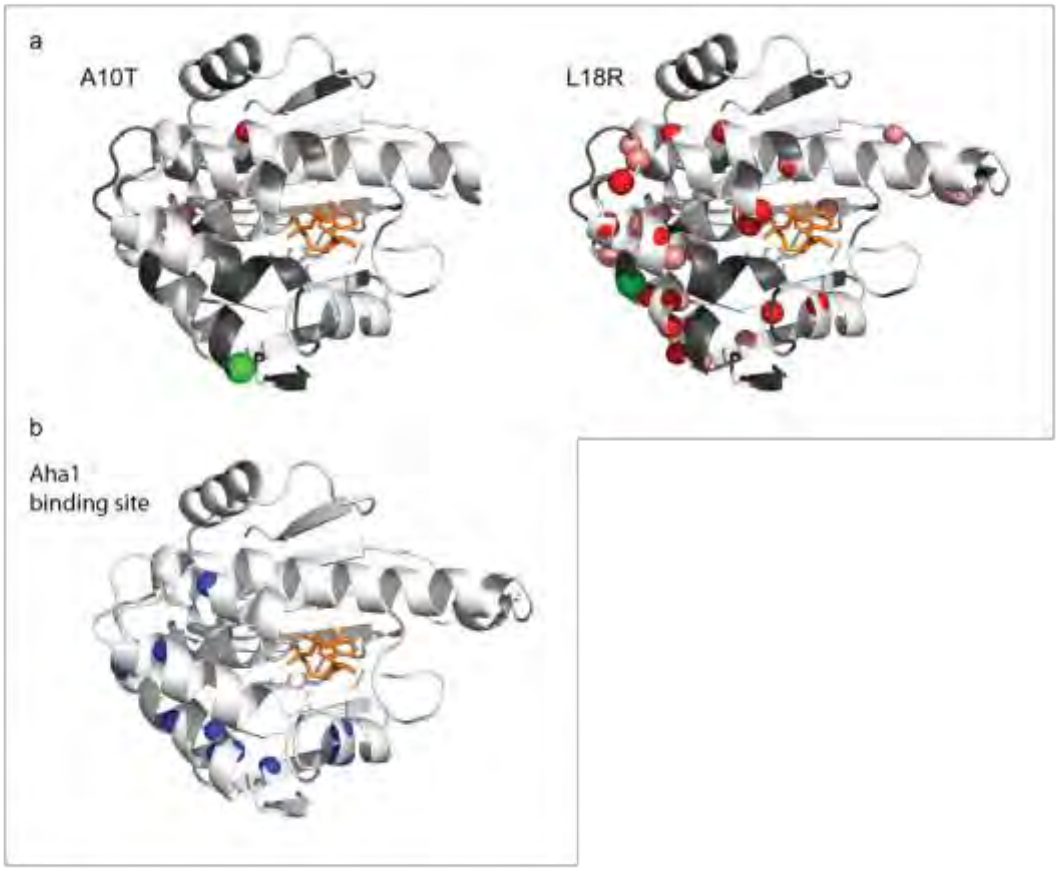

Supplementary Figure 3

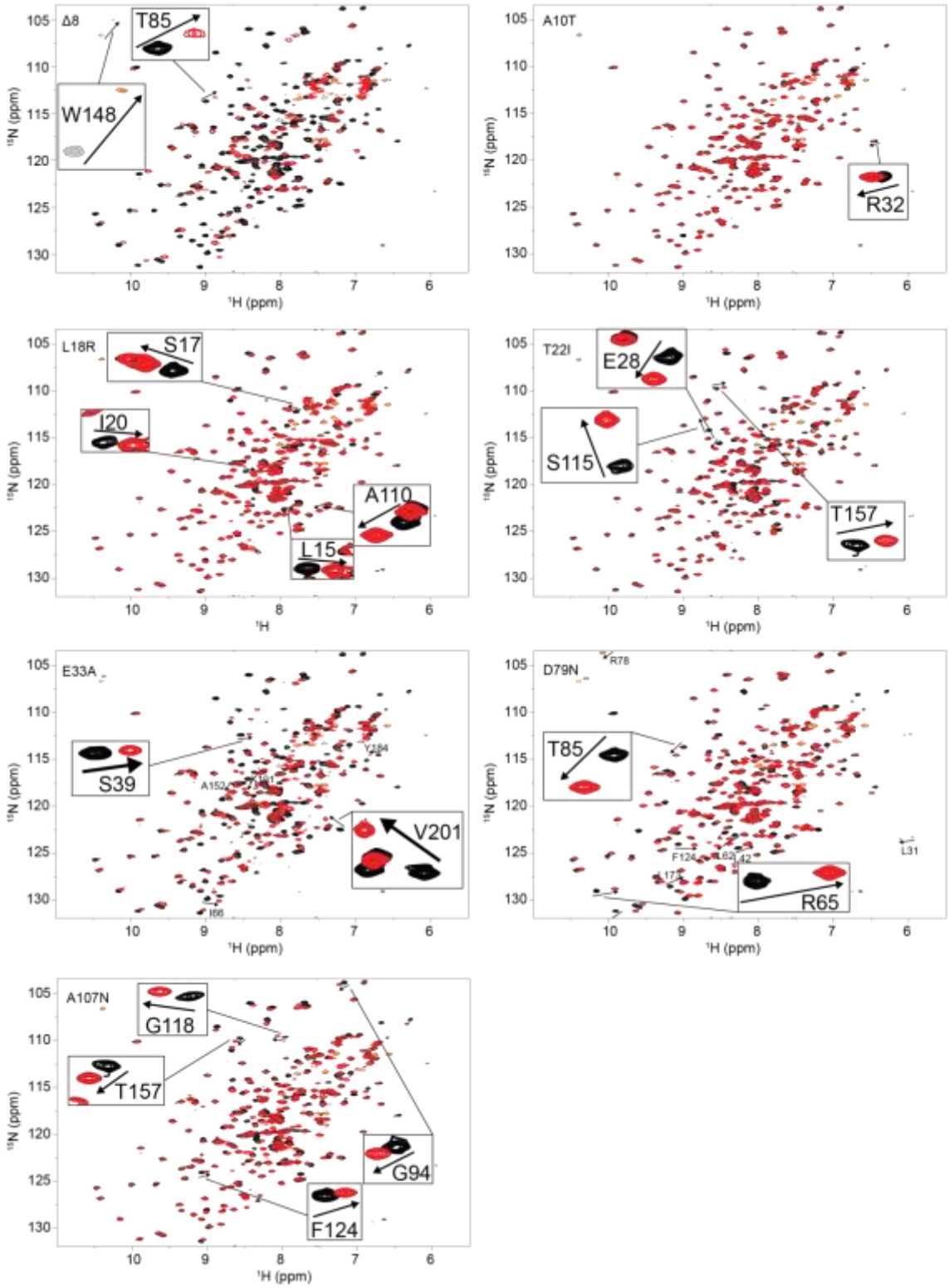

Supplementary Figure 4

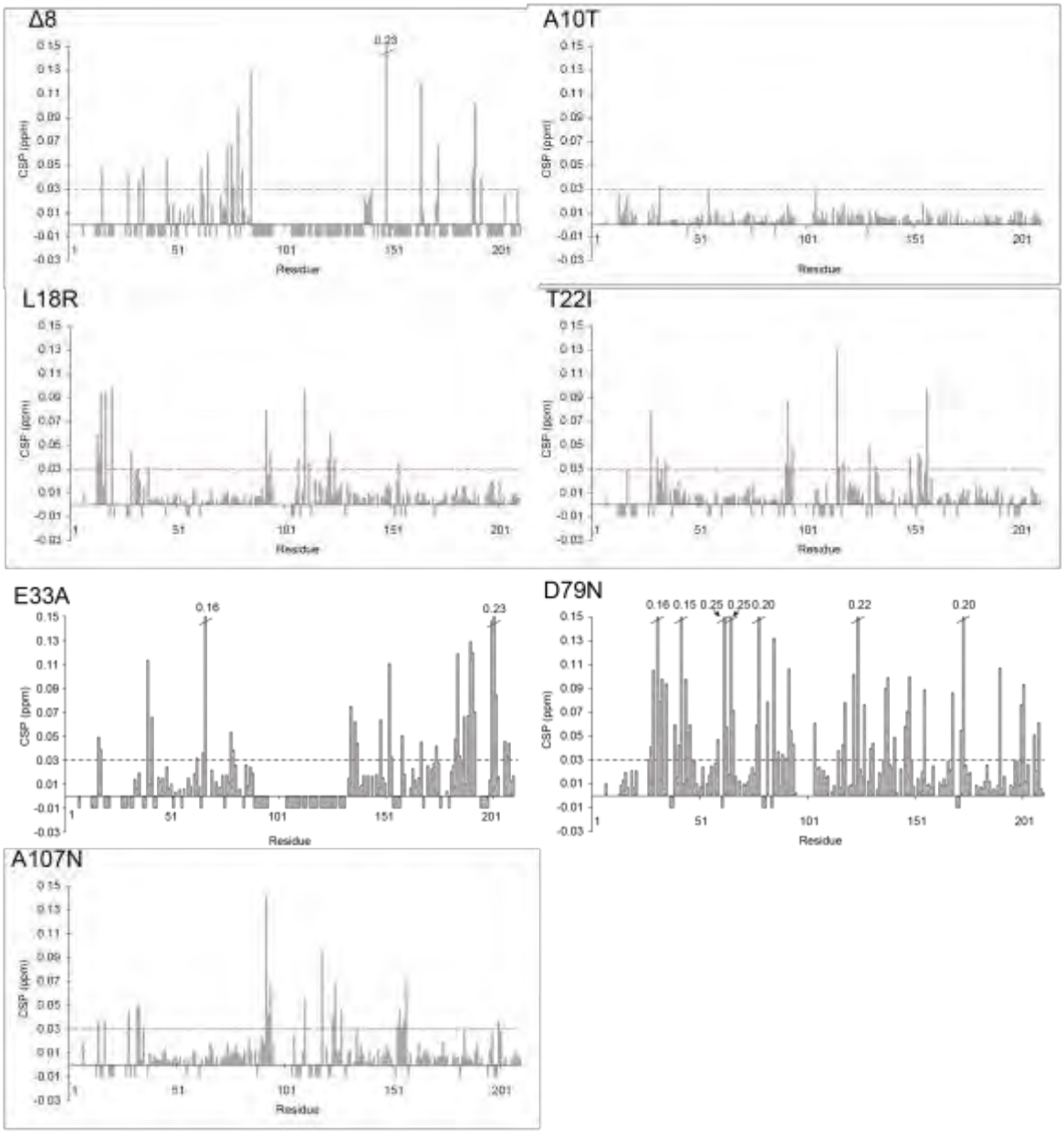

Supplementary Figure 5

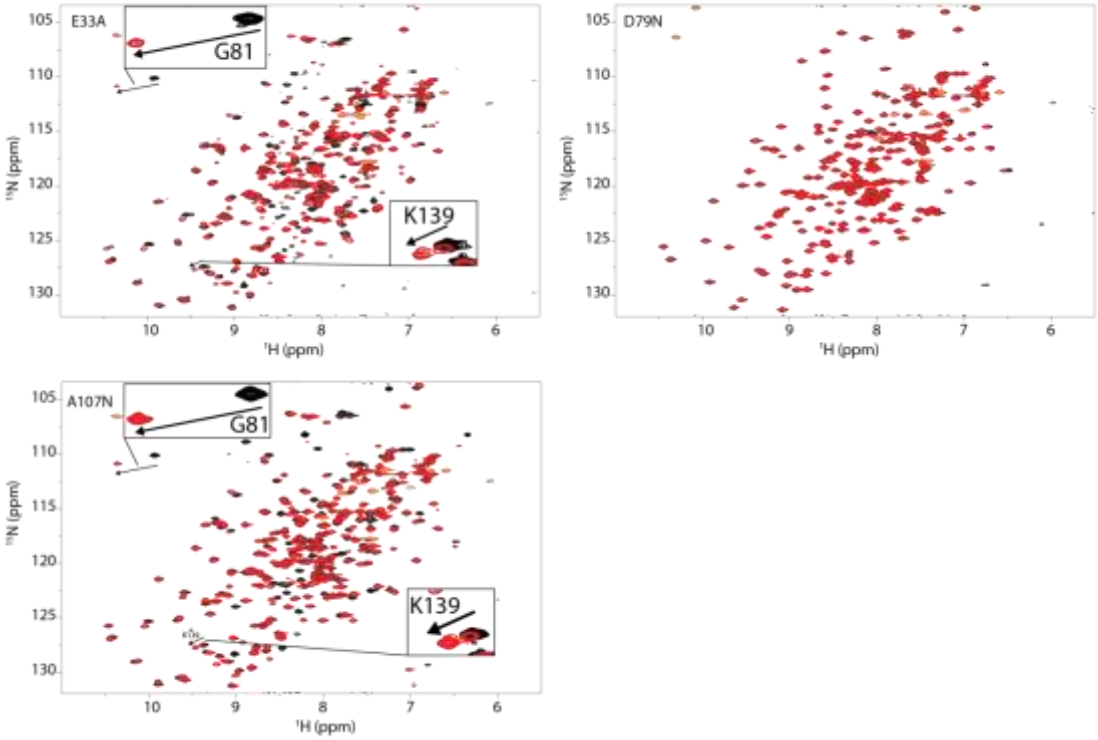

Supplementary Figure 6